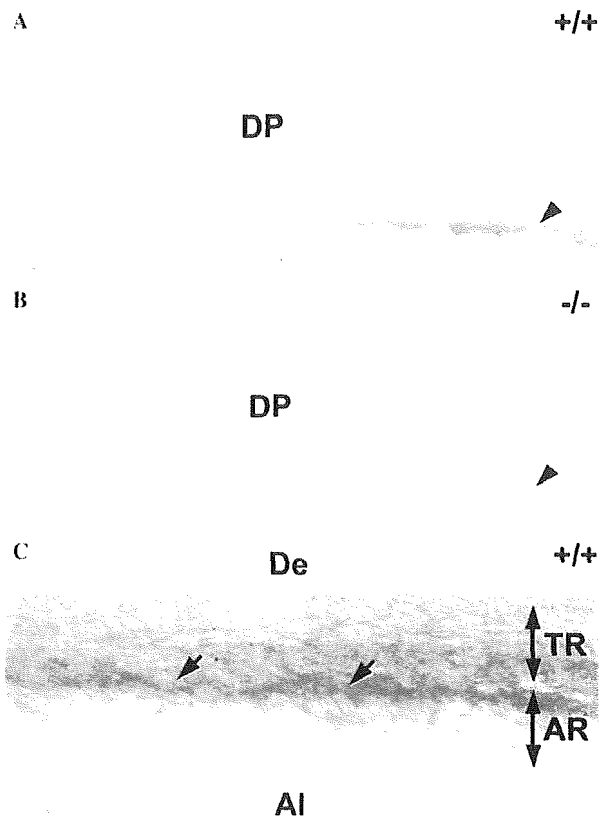

Fig. 4. Immunohistological localization of periostin protein in the periodontal ligament. Immuno-localization of periostin in the periodontal ligament of incisors (A,C) from 12-week-old wild-type (A,C) and *periostin*$^{-/-}$ (B) mice. The specific immunoreactivity for periostin is seen in the wild-type periodontal ligament (A, arrowhead), whereas *periostin*$^{-/-}$ mice have no expression of periostin protein there at all (B, arrowhead). Arrows in (C) indicate the shear zone, which is the boundary between the TR (tooth-related) and AR (alveolus-related) regions. Strong immunoreactivity for periostin is observed in the shear zone of the incisor periodontal ligament. DP, dental pulp; De, dentin; Al, alveolar bone.

in hematoxylin and eosin-stained sections from both the control 6- and the 12-week-old wild-type mice, and it appeared as a line when observed by microscopy (Figs. 5A and C, arrows). In the 6-week-old *periostin*$^{-/-}$ mice, the line in the shear zone was obscure (Fig. 5B). Notably, in the 12-week-old *periostin*$^{-/-}$ mice, the shear zone was completely disappeared, and the periodontal ligament was wider than that of the wild-type mice (Fig. 5D).

To examine the ultrastructure of the shear zone in the *periostin*$^{-/-}$ mice, we carried out electron-microscopic examination of the periodontal ligament around the incisors. In the 12-week-old wild-type mice, we observed the presence of fragmented collagen fibrils extracellularly (Fig. 5E), suggesting digestion of collagen fibrils in the shear zone. In contrast, in the *periostin*$^{-/-}$ mice, abundant intact collagen fibrils occupied the shear zone, and the line disappeared (Fig. 5F). These results suggest that *periostin* is required for the digestion process of collagen fibrils in the shear zone.

Periostin protein localized to collagen fibrils

To understand the molecular mechanism leading to formation of the shear zone, we focused on the extracellular matrix localization of periostin protein, because periostin is known to be localized in the boundary between the cells and extracellular matrix [12–14].

To investigate the extracellular matrix localization of periostin in the periodontal ligament in vivo, we conducted immuno-electron microscopic analysis using anti-periostin antibodies. Our results showed that the immuno-reactivity was detected mainly on the extracellular collagen fibrils, suggesting a possible interaction between periostin protein and collagen fibrils (Figs. 6A and B).

Discussion

In this study based on observations on *periostin*$^{-/-}$ mice, we show that *periostin* is required for formation of the shear zone in the periodontal ligament of incisors. Although several MMPs are involved in remodeling of the periodontal ligament in the previous studies [3–7], the molecular biological aspect of the shear zone is not studied well. The present study showed that periostin protein localized to the shear zone and interacted to the collagen fibrils. Since it was reported that remodeling of collagens predominantly occurs in the shear zone [9], our findings suggest that periostin protein plays a role in remodeling of collagen matrix.

Our electron microscopic analysis in the wild-type mice demonstrated that the digestion of collagen fibers occurred in the shear zone, suggesting that digestion of collagen fibers in this zone may be necessary for an appropriate eruption of incisors. However, in the *periostin*$^{-/-}$ mice, the same observation showed existence of abundant collagen fibers in the intercellular spaces and few digested ones compared with the wild-type littermates. The collagen fibers detected in the periodontal ligament of the *periostin*$^{-/-}$ mice appeared to connect the cementum to the alveolar bone tightly. This tight connection may have prevented the eruption of incisors in the *periostin*$^{-/-}$ mice.

In the *periostin*$^{-/-}$ mice, the defective remodeling in the periodontal ligament of the incisors became more severe as the animals aged. This observation indicates that no remodeled and metabolized extracellular matrices are accumulated to form an abnormal ligament as the animals aged in the absence of *periostin*.

Because disruption of the *periostin* gene caused the accumulation of undigested collagen fibers, periostin may be connected with the digestion of collagen fibers in the shear zone. In the shear zone, the movement between the tooth- and alveolus-related parts causes mechanical stress, and periodontal fibroblasts must sense and respond to this stress. In previous reports, expression of periostin was increased under the mechanically stressful condition of orthodontic tooth movement [17], and decreased by occlusal hypofunction in the mouse periodontal ligament [18].

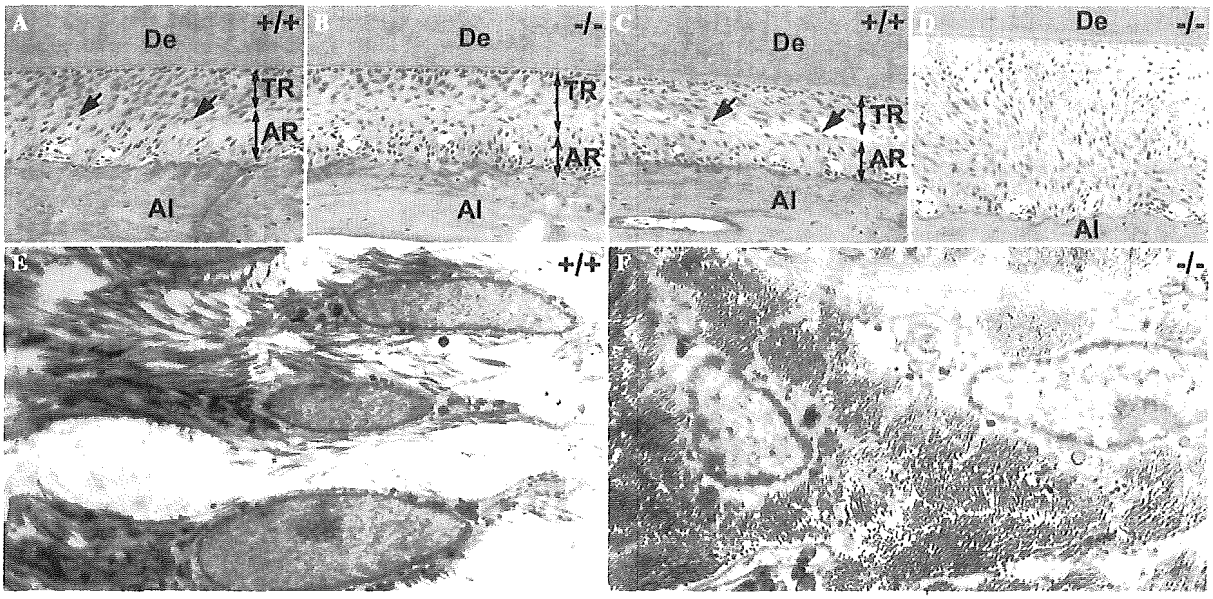

Fig. 5. Remodeling of the periodontal ligament of incisors is defective in periostin $^{-/-}$ mice. Histological micrographs (hematoxylin/eosin staining) of the periodontal ligament from 6-week- (A,B) and 12-week- (C,D) old wild-type (+/+) and periostin $^{-/-}$ (−/−) mice. Arrows indicate the shear zone, which is the boundary between the TR (tooth-related) and AR (alveolus-related) regions. The shear zone in wild-type mice (A,C) is clearly distinguishable, whereas it is obscure in 6-week-old periostin $^{-/-}$ mice (B) and is completely absent in 12-week-old periostin $^{-/-}$ mice (D). Electron microscopy of the incisor periodontal ligament shows evidence of digestion of collagen fibers in 12-week-old wild-type mice (E), but undigested and abundant collagen bundles in 12-week-old periostin $^{-/-}$ mice (F). DP, dental pulp; En, enamel; De, dentin; Al, alveolar bone; TR, tooth-related region; and AR, alveolus-related region.

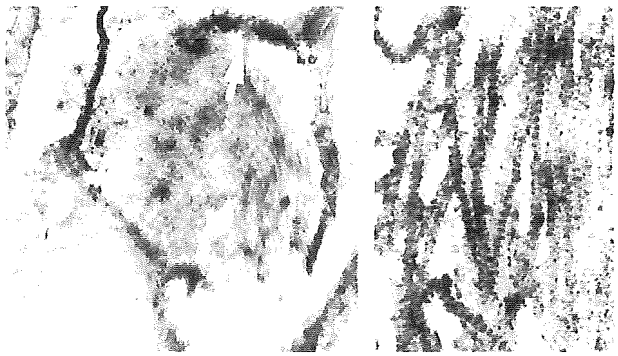

Fig. 6. Immuno-electron microscopic analysis for periostin. Immunoreactivity for periostin is observed in the boundary between cells and the extracellular matrix in the periodontal ligament of the wild-type mice (A, arrows). At a high magnification of the collagen fibers, periostin is seen to be associated with the collagen fibers (B).

These results indicate that in the shear zone, mechanical stress caused by the movement of tooth-related parts may increase the expression of periostin in the shear zone.

The *periostin*$^{-/-}$ mice showed abnormal appearance of incisors, especially disorganized enamel layers and compressed and undulated dentin layers. The present study demonstrates the specific function of periostin in the shear zone. We concluded that the incisors of the *periostin*$^{-/-}$ mice were continuously built in the apical region, but could not erupt because of the defective remodeling of the periodontal ligament, therefore, demonstrating the compressed appearance of the enamel and dentin of their incisors.

However, there is one question whether *periostin* is involved in formation of the enamel and dentin, and affects the functions of the ameloblast and odontoblast directly. In the ameloblastic layer and the apical bud, expression of periostin is barely observed. Periostin localized to the periodontal ligament specifically in the incisors of mice, suggesting that the function of periostin may be restricted to the periodontal ligament.

Our recent findings indicate that periostin protein binds directly to type I collagen in vitro (Shimazaki et al., manuscript in preparation). Periostin protein in the periodontal ligament was associated with the collagen fibers in vivo. These results suggest that periostin protein in vivo binds to type I collagen fibers directly. Periostin is a member of the fasciclin I family, whose members include β ig-h3 protein [10]. It has been reported that β ig-h3 also binds to collagens directly [19,20]. Our results and these previous reports suggest a common function between periostin and β ig-h3 proteins. Furthermore, periostin acts as a cell spreading factor for fibroblastic cells [12,21] and is reported as a ligand for integrin αVβ3 or αVβ5 [21–23]; and its four Fas I domains are postulated to be a binding domain for integrin from the results of biochemical analysis of β ig-h3 [24,25]. These findings imply the existence of a collagen–periostin–integrin complex in the shear zone.

Periostin is a highly conserved protein among various species such as human, dog, rat, mouse, chick, and zebrafish (data not shown). Zebrafish periostin is required for formation of the myoseptum, which is composed of dense collagens [26]. The myoseptum is a connective tissue

layer that divides the somites from the trunk [27]. The structure and function of the myoseptum are similar to those of the mammalian tendon. Both the myoseptum and tendon serve as the transmitter of muscular contractility to bones and adjoining muscles, and their structures are indispensable for movement of vertebrate animals. The tendon is also composed of dense collagen fibers, and is exposed to mechanical stress caused by physical exercise, just as are the periodontal ligament and the periosteum [28,29]. Furthermore, expression of mouse periostin is also found in tendons [13]. Tissues that are exposed to strong mechanical stress form a dense collagenous extracellular matrix, and this matrix is remodeled sufficiently to tolerate the stress when the tissues are deformed by strong mechanical stress beyond the permissible range. These previous findings and our present results suggest that periostin is responsible for triggering the remodeling of collagenous tissues.

To our knowledge, this is the first report on a molecule responsible for formation of the shear zone. The periodontal ligament in humans is also responsible for the eruption and realignment of teeth. The *periostin* is a gene whose sequence is highly conserved between mice and humans [10], and periostin protein was also detected in the human periodontal ligament (unpublished results). Therefore, *periostin*$^{-/-}$ mice provide a novel model system to evaluate the cause of eruption disturbance and malocclusion in humans.

Acknowledgments

We thank A. Moriyama, Y. Nakatani, and M. Shimazaki for critical reading of the manuscript; E. Ikeno for technical assistance in the generation of *periostin*$^{-/-}$ mice; Y. Hattori for technical assistance in protein purification; M. Ikumi, T. Nishiyama, Y. Nagano, and K. Kume for the maintenance and manipulation of the animals; H. Tanabe, A. Oshima, and K. Horiuchi for their technical advice. This work was supported by grants from the Promotion of Niigata University Research Project and from the Ministry of Education, Sports, Science and Technology.

References

[1] P. Lekic, J. Rojas, C. Birek, H. Tenenbaum, C.A. McCulloch, Phenotypic comparison of periodontal ligament cells in vivo and in vitro, J. Periodontal Res. 36 (2001) 71–79.

[2] B.K. Berkovitz, Periodontal ligament: structural and clinical correlates, Dent. Update 31 (2004) 46–50, pp. 52, 54.

[3] V. Everts, E. van der Zee, L. Creemers, W. Beertsen, Phagocytosis and intracellular digestion of collagen, its role in turnover and remodelling, Histochem. J. 28 (1996) 229–245.

[4] M.T. van der Pauw, T. Van den Bos, V. Everts, W. Beertsen, Phagocytosis of fibronectin and collagens type I, III, and V by human gingival and periodontal ligament fibroblasts in vitro, J. Periodontol. 72 (2001) 1340–1347.

[5] I. Takahashi, M. Nishimura, K. Onodera, J.W. Bae, H. Mitani, M. Okazaki, Y. Sasano, Expression of MMP-8 and MMP-13 genes in the periodontal ligament during tooth movement in rats, J. Dent. Res. 82 (2003) 646–651.

[6] M. Tsubota, Y. Sasano, I. Takahashi, M. Kagayama, H. Shimauchi, Expression of MMP-8 and MMP-13 mRNAs in rat periodontium during tooth eruption, J. Dent. Res. 81 (2002) 673–678.

[7] A.L. Bolcato-Bellemin, R. Elkaim, A. Abehsera, J.L. Fausser, Y. Haikel, H. Tenenbaum, Expression of mRNAs encoding for alpha and beta integrin subunits, MMPs, and TIMPs in stretched human periodontal ligament and gingival fibroblasts, J. Dent. Res. 79 (2000) 1712–1716.

[8] W. Beertsen, V. Everts, A. van den Hooff, Fine structure and possible function of cells containing leptomergic organelles in the periodontal ligament of the rat incisor, Arch. Oral Biol. 19 (1974) 1099–1100.

[9] W. Beertsen, V. Everts, The site of remodeling of collagen in the periodontal ligament of the mouse incisor, Anat. Rec. 189 (1977) 479–497.

[10] S. Takeshita, R. Kikuno, K. Tezuka, E. Amann, Osteoblast-specific factor 2: cloning of a putative bone adhesion protein with homology with the insect protein fasciclin I, Biochem. J. 294 (Pt. 1) (1993) 271–278.

[11] T. Sugiura, H. Takamatsu, A. Kudo, E. Amann, Expression and characterization of murine osteoblast-specific factor 2 (OSF-2) in a baculovirus expression system, Protein Expr. Purif. 6 (1995) 305–311.

[12] K. Horiuchi, N. Amizuka, S. Takeshita, H. Takamatsu, M. Katsuura, H. Ozawa, Y. Toyama, L.F. Bonewald, A. Kudo, Identification and characterization of a novel protein, periostin, with restricted expression to periosteum and periodontal ligament and increased expression by transforming growth factor beta, J. Bone Miner. Res. 14 (1999) 1239–1249.

[13] Y. Hirose, H. Suzuki, N. Amizuka, J. Shimomura, Y. Kawano, K. Nozawa-Inoue, A. Kudo, T. Maeda, Immunohistochemical localization of periostin in developing long bones of mice, Biomed. Res. 24 (2003) 31–37.

[14] H. Suzuki, N. Amizuka, I. Kii, Y. Kawano, K. Nozawa-Inoue, A. Suzuki, H. Yoshie, A. Kudo, T. Maeda, Immunohistochemical localization of periostin in tooth and its surrounding tissues in mouse mandibles during development, Anat. Rec. (2004).

[15] I. Kii, N. Amizuka, S. Kitajima, M. Li, K. Takeuchi, T. Maeda, J. Kanno, T. Inoue, Y. Saga, A. Kudo, Mechanical stress dependent remodeling of the periodontal ligament is defective in periostin deficient mice: mechanotransduction through periostin protein, J. Bone Miner. Res. 19 (Suppl. 1) (2004) s21.

[16] N. Amizuka, H.S. Lee, M.Y. Kwan, A. Arazani, H. Warshawsky, G.N. Hendy, H. Ozawa, J.H. White, D. Goltzman, Cell-specific expression of the parathyroid hormone (PTH)/PTH-related peptide receptor gene in kidney from kidney-specific and ubiquitous promoters, Endocrinology 138 (1997) 469–481.

[17] J. Wilde, M. Yokozeki, K. Terai, A. Kudo, K. Moriyama, The divergent expression of periostin mRNA in the periodontal ligament during experimental tooth movement, Cell Tissue Res. 312 (2003) 345–351.

[18] E. Afanador, M. Yokozeki, Y. Oba, Y. Kitase, T. Takahashi, A. Kudo, K. Moriyama, Messenger RNA expression of periostin and Twist transiently decrease by occlusal hypofunction in mouse periodontal ligament, Arch. Oral Biol. 50 (2005) 1023–1031.

[19] E. Hanssen, B. Reinboth, M.A. Gibson, Covalent and non-covalent interactions of betaig-h3 with collagen VI. Beta ig-h3 is covalently attached to the amino-terminal region of collagen VI in tissue microfibrils, J. Biol. Chem. 278 (2003) 24334–24341.

[20] K. Hashimoto, M. Noshiro, S. Ohno, T. Kawamoto, H. Satakeda, Y. Akagawa, K. Nakashima, A. Okimura, H. Ishida, T. Okamoto, H. Pan, M. Shen, W. Yan, Y. Kato, Characterization of a cartilage-derived 66-kDa protein (RGD-CAP/beta ig-h3) that binds to collagen, Biochim. Biophys. Acta 1355 (1997) 303–314.

[21] L. Gillan, D. Matei, D.A. Fishman, C.S. Gerbin, B.Y. Karlan, D.D. Chang, Periostin secreted by epithelial ovarian carcinoma is a ligand for alpha(V)beta(3) and alpha(V)beta(5) integrins and promotes cell motility, Cancer Res. 62 (2002) 5358–5364.

[22] R. Shao, S. Bao, X. Bai, C. Blanchette, R.M. Anderson, T. Dang, M.L. Gishizky, J.R. Marks, X.F. Wang, Acquired expression of periostin by human breast cancers promotes tumor angiogenesis through up-regulation of vascular endothelial growth factor receptor 2 expression, Mol. Cell. Biol. 24 (2004) 3992–4003.

[23] S. Bao, G. Ouyang, X. Bai, Z. Huang, C. Ma, M. Liu, R. Shao, R.M. Anderson, J.N. Rich, X.F. Wang, Periostin potently promotes metastatic growth of colon cancer by augmenting cell survival via the Akt/PKB pathway, Cancer Cell 5 (2004) 329–339.

[24] J.E. Kim, S.J. Kim, B.H. Lee, R.W. Park, K.S. Kim, I.S. Kim, Identification of motifs for cell adhesion within the repeated domains of transforming growth factor-beta-induced gene, betaig-h3, J. Biol. Chem. 275 (2000) 30907–30915.

[25] J.E. Kim, H.W. Jeong, J.O. Nam, B.H. Lee, J.Y. Choi, R.W. Park, J.Y. Park, I.S. Kim, Identification of motifs in the fasciclin domains of the transforming growth factor-beta-induced matrix protein betaig-h3 that interact with the alphavbeta5 integrin, J. Biol. Chem. 277 (2002) 46159–46165.

[26] H. Kudo, N. Amizuka, K. Araki, K. Inohaya, A. Kudo, Zebrafish periostin is required for the adhesion of muscle fiber bundles to the myoseptum and for the differentiation of muscle fibers, Dev. Biol. 267 (2004) 473–487.

[27] G.M. Dubois, Z. Haftek, C. Crozet, R. Garrone, D. Le Guellec, Structure and spatio temporal expression of the full length DNA complementary to RNA coding for alpha2 type I collagen of zebrafish, Gene 294 (2002) 55–65.

[28] A.P. Summers, T.J. Koob, The evolution of tendon–morphology and material properties, Comp. Biochem. Physiol. A Mol. Integr. Physiol. 133 (2002) 1159–1170.

[29] T.J. Koob, A.P. Summers, Tendon–bridging the gap, Comp. Biochem. Physiol. A Mol. Integr. Physiol. 133 (2002) 905–909.

J Toxicol Pathol 2005; 18: 41–46

Original

Electron Microscopical Evidence of the Protective Function of Thioredoxin (TRX/ADF) Transgene against 2,3,7,8-tetrachlorodibenzo-*p*-dioxin (TCDD)-induced Cellular Toxicity in the Liver and Brain

Byung-Il Yoon[1,5], Toyozo Kaneko[1], Yoko Hirabayashi[1], Takayoshi Imazawa[2], Akiyoshi Nishikawa[2], Yukio Kodama[1], Jun Kanno[1], Junji Yodoi[4], Jeong-Hee Han[5], Masao Hirose[2], and Tohru Inoue[3]

[1]Division of Cellular and Molecular Toxicology
[2]Department of Pathology
[3]Safety and Research Center of National Institute of Health Sciences, Tokyo 158–8501, Japan
[4]Department of Biological Responses, Institute for Virus Research, Kyoto University, Kyoto, Japan
[5]Department of Veterinary Medicine, Kangwon National University, Chunchcon 200–701, Korea

Abstract: The present study was performed to assess the protective role of thioredoxin/adult T-cell leukemia-derived factor (TRX/ADF) on the liver and brain cell damages induced by 2,3,7,8-tetrachlorodibenzo-*p*-dioxin (TCDD) in ADF wild-type (WT) and transgenic (Tg) mice. The ADF WT and Tg mice were intraperitoneally injected with a single dose of TCDD (150 μg/kg body weight). One day after the treatment, the liver and brain tissues were examined electron microscopically to evaluate the cellular toxicity. In the ADF WT mice, marked reduction of subcellular components, such as mitochondria, rough endoplasmic reticula, and glycogen granules, as well as swelling of the remaining mitochondria, were evident in the liver cells. However, attenuation of these changes was evident in TCDD-treated TRX/ADF mice. Similar subcellular changes noted in the neuronal cells of TCDD-treated WT mice were also attenuated in Tg mice. The results suggest that oxidative cellular damage contributes to the acute toxicity induced by TCDD and that TRX/ADF protects against it. (J Toxicol Pathol 2005; **18**: 41–46)

Key words: Ah receptor, brain, liver, 2,3,7,8-tetrachlrodibenzo-*p*-dioxin (TCDD), thioredoxin/adult T-cell leukemia-derived factor (TRX/ADF), transgenic (Tg) mouse

Introduction

As one of the aromatic hydrocarbons, 2,3,7,8-tetrachlorodibenzo-*p*-dioxin (TCDD) is a widely spread environmental pollutant that has a broad spectrum of toxic effects on a variety of tissues such as the thymus, liver, testes and central nervous system in mammals[1–6]. Although a number of studies have shown that the toxic effects of TCDD are mediated by intracytoplasmic aromatic hydrocarbon receptor (AhR)[7–9], the toxic mechanism of TCDD on the target organs is still not fully understood. Among the toxic events, oxidative stress is considered to play a major role in the toxic mechanism of TCDD, as characterized by marked increases of lipid peroxidation, the formation of reactive oxygen species, and DNA single-strand break[9–14].

Exogenous xenobiotics, such as aromatic hydrocarbons, result in profound induction of cytochrome P450 enzymes in the liver, resulting in the generation of reactive oxygen species[15,16]. On the other hand, the brain is rich in peroxidizable fatty acids and has relatively low catalase activity[17]. Therefore, these organs are considered to be highly susceptible to oxidative stresses[18]. In fact, the contribution of oxidative stress in TCDD-induced cellular damage of the liver and brain has been suggested in previous studies[13,18–22].

Adult T-cell leukemia-derived factor (ADF) is a human thioredoxin (TRX) associated with the reduction/oxidation (redox) regulation of the cellular environment[23]. TRX/ADF is a stress-inducible protein and its expression is up-regulated after viral infection as well as in cellular stress conditions induced by oxidative agents such as hydrogen peroxide or diamide, irradiation with X-rays and ultraviolet

Received: 24 September 2004, Accepted: 15 February 2005
Mailing address: Byung-Il Yoon, Department of Veterinary Medicine, College of Animal Resources Sciences, Kangwon National University, 192–1 Hyoja2-dong, Chunchcon, Kangwon 200–701, Republic of Korea
TEL: 82-33-250-8679 FAX: 82-33-244-2367
E-mail: byoon@kangwon.ac.kr

light, or ischemic reperfusion[23]. Previous studies have shown that TRX/ADF plays a role in the cellular defense mechanism against oxidative cellular damage via the regulation of intracellular redox status, since exogenously administered TRX/ADF protected cells from oxidative cellular injury[24,25].

We recently reported for the first time the protective function of TRX/ADF against TCDD-induced hematotoxicity in ADF transgenic (Tg) mice, indicating oxidative stress contributes to the hematotoxic mechanism of TCDD[26]. We hypothesized in the present study that overexpression of TRX/ADF might also be effective for protection against the toxic effects of TCDD on the liver and brain tissues in which oxidative stress has also been implicated in the toxic mechanism. For this purpose, we injected TCDD with a dosage capable of inducing oxidative stress in the liver following acute exposure[21], to ADF wild-type (WT) and transgenic (Tg) mice, and then compared subcellular changes electron microscopically in the liver and brain tissues.

Materials and Methods

Animals

TRX/ADF overexpressed mice (ADF Tg mice), originally produced by Dr. A. Mitsui[27], were maintained in a laboratory facility with a 12:12-hour light-dark cycle at an ambient temperature of 21 ± 2°C at the National Institute of Health Sciences (NIHS) of Japan by breeding ADF WT and Tg mice. Animals were screened by PCR of their tail DNA to determine their genotypes. At 8 weeks of age, male ADF WT and Tg mice (23.5–24.8 g) were transferred to a vinyl isolator established in a hazard room designed to prevent contamination from the outside environment and randomly allocated within the same genotype to housing with 6 animals per cage. A pelleted basal diet (CRF-1; Funabashi Farm, Funabashi, Japan) and tap water were provided *ad libitum* throughout the study.

Chemical

TCDD was obtained from Radian International, Cambridge Isotope Laboratories, Inc. (Andover, MA, USA; purity: 98 %). TCDD was initially dissolved in a small volume of acetone and subsequently adjusted to the concentration of 10 μg/ml in olive oil.

Experimental design

ADF WT and Tg mice were divided into vehicle controls and TCDD treatment groups, each consisting of 6 animals. After one week of acclimation, TCDD at 150 μg/kg was intraperitoneally injected once to animals of treatment groups, and the corresponding volume of olive oil was similarly injected to vehicle controls. The dosage of TCDD was selected based on previous study results that showed oxidative stress in the liver was induced by a single bolus injection to mice[21]. One day after the treatment, the animals were sacrificed by decapitation and then examined grossly. The liver and brain were then excised and their weights were measured.

The animal protocol was reviewed and approved by the Animal Care and Use Committee of the NIHS, Japan.

Morphological assessment

For histological examination, liver tissues in all animals were fixed in 10% neutral buffered formalin (pH 7.4). After routine processing, the paraffin-embedded sections were stained with hematoxylin and eosin and then examined histopathologically under a light microscope.

For electron microscopical examination, tissue specimens from the liver and cerebral cortex were respectively prepared from three animals each of the control and treatment groups of ADF WT and Tg mice. Small tissue blocks, sized 1 mm^3, were fixed with 2.5% glutaraldehyde in 0.2 M Sorenson's sodium phosphate buffer, pH 7.2, for 8 hours at 4°C. After washing with 0.1 M PBS (pH 7.4), the tissues were post-fixed with 1% osmium tetroxide for 90 minutes. After washing in 0.1 M PBS, the tissues were dehydrated with ethanol and propylene oxide and then embedded in Epon 812. Ultrathin sections were double-stained with uranyl acetate and lead citrate. The sections were examined with JEOL-1200 EX II electron microscope (JEOL, Tokyo, Japan).

Results

After one day of TCDD treatment, absolute liver weight had decreased to 71.4% of the vehicle control group in ADF WT mice and 83.2% in ADF Tg mice (data not shown).

Histologically, apoptotic liver cell debris and also focal liver cell necrosis were sparsely observed in the centrilobular areas of both TCDD-treated WT and ADF Tg mice, without showing apparent difference in the severity between genotypes (data not shown). Vehicle control animals did not show such liver cell changes in either genotype.

Electron microscopically, liver cells of the WT mice treated with TCDD exhibited a prominent decrease of cytoplasmic glycogen granules and rough endoplasmic reticula (RERs) and an increase of smooth endoplasmic reticula (SERs) (Fig. 1B). The number of mitochondria was also decreased and the remaining mitochondria showed swelling with disorganized cristae and lucent matrix. Increased fat droplets were also evident in the cytoplasm of less affected hepatocytes. On the other hand, transgene of Trx/ADF notably attenuated these morphological changes following TCDD treatment (Fig. 1C). In the cerebral cortex, neuronal cells showed a decrease in the number of RERs, ribosomes and mitochondria in WT mice treated with TCDD (Fig. 2B) but not in ADF Tg mice treated similarly with TCDD (Fig. 2C). Vehicle control animals did not show such neuronal cell changes in either genotype.

Discussion

In the present study, acute treatment with TCDD

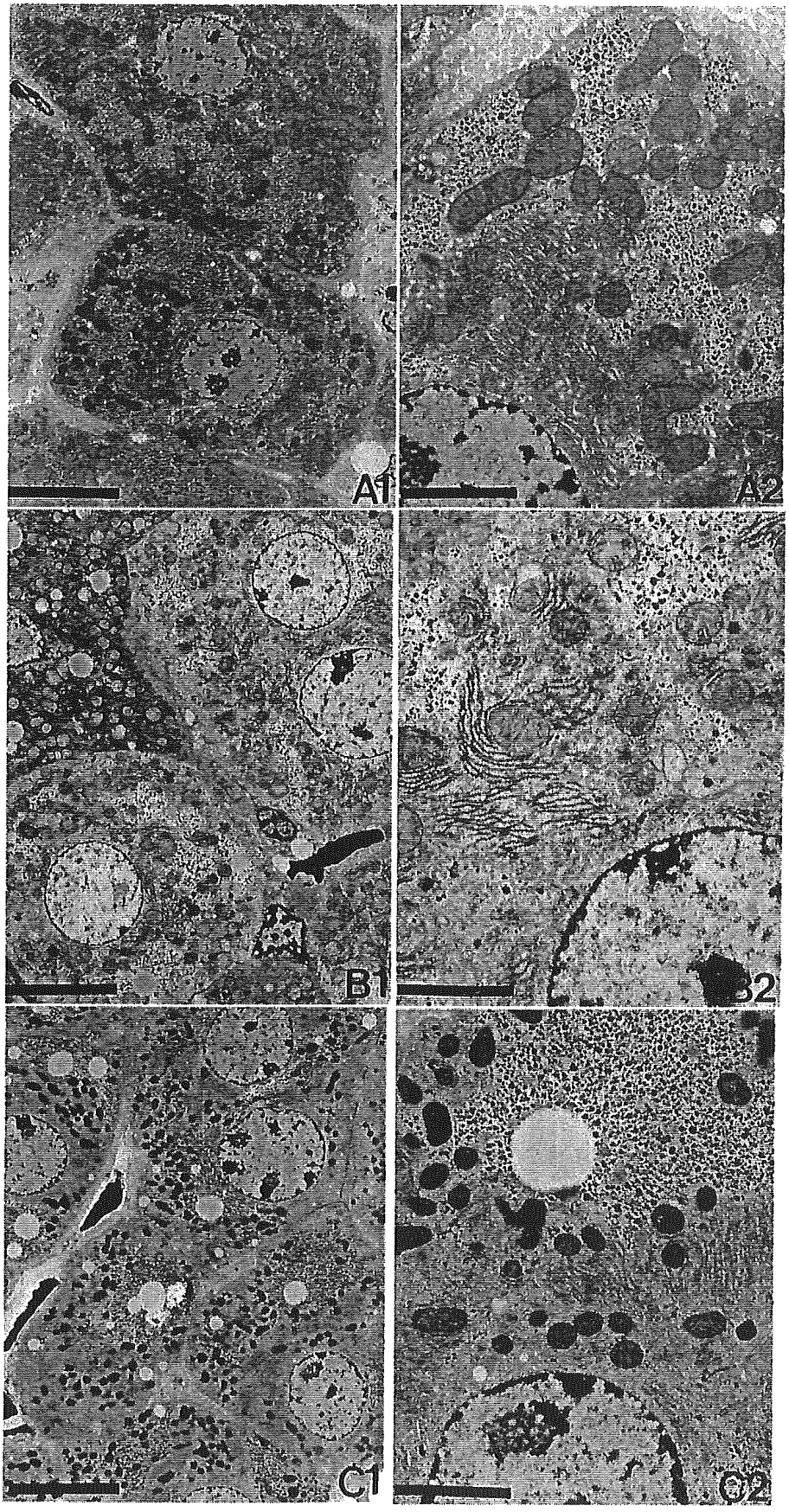

Fig. 1. Electron micrographs of liver cells from ADF WT and Tg mice treated with vehicle or TCDD. (A) Vehicle-treated ADF WT mouse, (B) TCDD-treated ADF WT mouse, and (C) TCDD-treated ADF Tg mouse. Note cytoplasmic swelling associated with a profound decrease of glycogen granules, RERs and mitochondria in the liver cells of the TCDD-treated ADF WT mouse (B). Swelling of the remaining mitochondria with disorganized cristae and lucent matrix is also evident (B). Attenuation of these morphological changes is evident in the TCDD-treated ADF Tg mouse (C). Uranyl acetate and lead citrate. Bar=10 μm (A1, B1, C1), Bar=3 μm (A2, B2, C2).

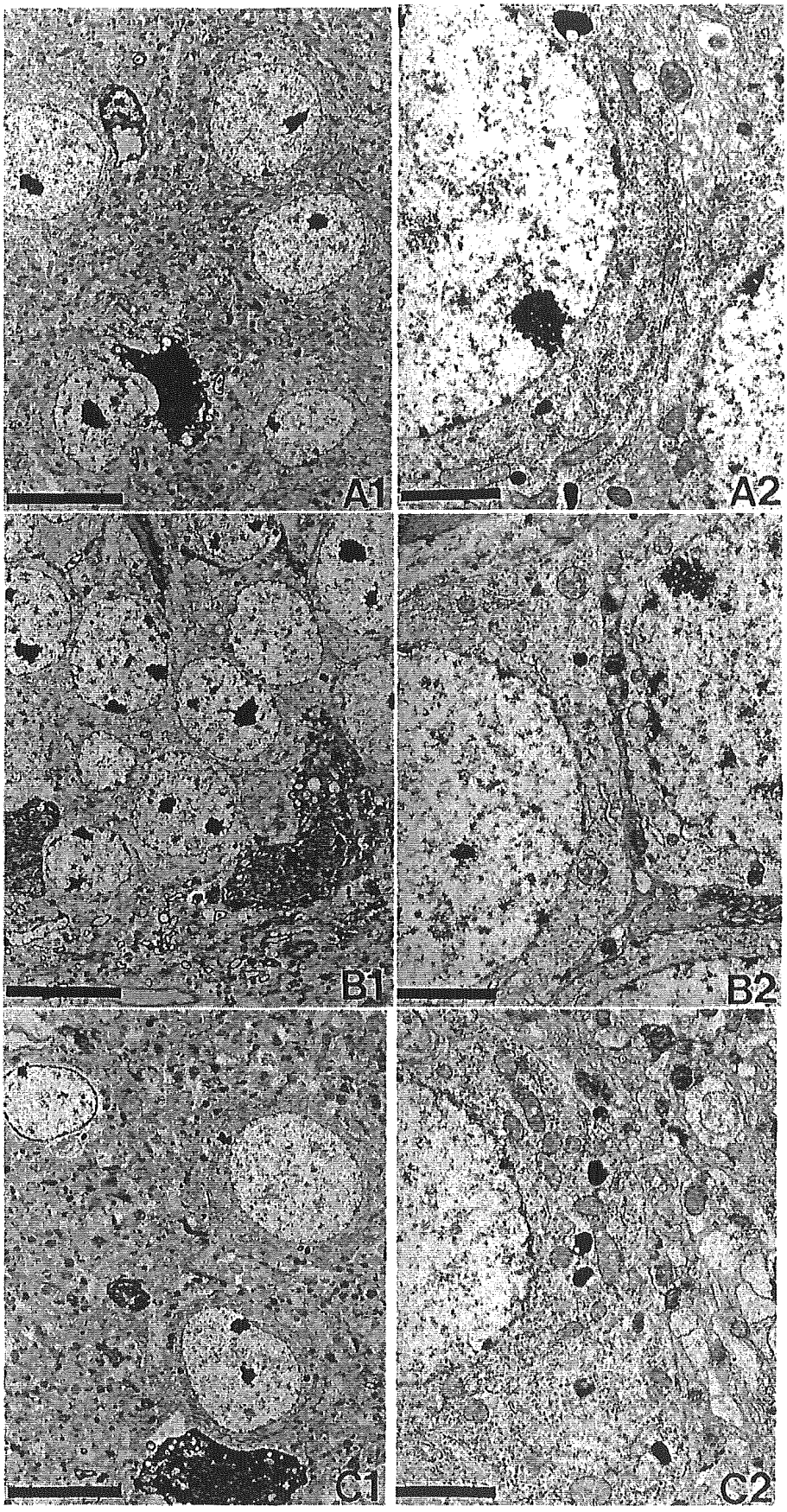

Fig. 2. Electron micrographs of neuronal cells in the cerebral cortex from ADF WT and Tg mice treated with vehicle or TCDD. (A) Vehicle-treated ADF WT mouse, (B) TCDD-treated ADF WT mouse, and (C) TCDD-treated ADF Tg mouse. Note the decrease of RER, ribosome and mitochondria in the cytoplasm of neuronal cells of the TCDD-treated ADF WT mouse (B). In the TCDD-treated ADF Tg mouse, mitochondrial swelling is also evident, but attenuation of the morphological changes can be seen, too. (C). Uranyl acetate and lead citrate. Bar=10 μm (A1, B1, C1), Bar=2 μm (A2, B2, C2).

induced ultrastructural alterations in the cytoplasmic components of liver cells characterized by prominent decrease of glycogen granules and RERs, proliferation of SERs, decrease and degradation of mitochondria, and increase of lipid droplets. These subcellular alterations were mostly consistent with those noted in the guinea pig liver following TCDD treatment[28], but concentric membrane arrays in the liver cells were not evident in the present study, presumably due to the different experimental protocol or the different species used in the studies. In the cerebral neuronal cells in the present study, alterations in subcellular components by TCDD were also evident, despite the changes being less profound than those in the liver cells. These subcellular changes in the liver and neuronal cells may represent the cytotoxic outcome of TCDD due to oxidative cellular damage and also cellular adaptation including detoxification.

Effective prevention of TCDD-induced toxicity by administration of antioxidants such as oltipraz[5-(2-pyrazinyl)-4-methyl-1,2-dithiol-3-thione] or butylated hydroxyanisole, or by pretreatment with vitamins A and E further supports the hypothesis that oxidative processes are involved in TCDD-induced toxicity[29,30]. Attenuation of subcellular changes in the liver and neuronal cells by transgene of TRX/ADF in the present study indicates the critical role of oxidative stress in the toxic events induced by TCDD, and also the protective function of ADF/TRX in these organs, as in our previous study of TCDD-induced bone marrow toxicity[26]. The protective effect of TRX/ADF against oxidative cellular damage is believed to be achieved by free radical scavengers[31], activation of DNA repair enzymes, such as activator protein endonuclease (Ref-1; redox factor-1)[32], and activation of nuclear factor-kappa B (NF-kB)[33].

Taken together, the results of our present study strongly suggest that the acute toxic effect induced in the liver and brain by a single large dose of TCDD is due to oxidative cellular damage, and that TRX/ADF plays a role in protection against TCDD-induced acute toxicity. Considering the routes and concentrations of TCDD exposed to humans, research on the effect of extremely low doses of TCDD by oral ingestion on the oxidative cellular damage of target organs is clearly warranted.

References

1. Kociba RJ, Keeler PA, Park CN, and Gehring PJ. 2,3,7,8-Tetrachlorodibenzo-*p*-dioxin (TCDD): results of a 13-week oral toxicity study in rats. Toxicol Appl Pharmacol. **35**: 553–574. 1976.
2. Chahoud I, Krowke R, Schimmel A, Merker HJ, and Neubert D. Reproductive toxicity and pharmacokinetics of 2,3,7,8-tetrachlorodibenzo-*p*-dioxin. 1. Effects of high doses on the fertility of male rats. Arch Toxicol. **63**: 432–439. 1989.
3. Funseth E and Ilbäck N-G. Effects of 2,3,7,8-tetrachlorodibenzo-*p*-dioxin on blood and spleen natural killer (NK) cell activity in the mouse. Toxicol Lett. **60**: 247–256. 1992.
4. Ivens IA, Loser E, Rinke M, Schmidt U, and Neupert M. Toxicity of 2,3,7,8-tetrachlorodibenzo-*p*-dioxin in rats after single oral administration. Toxicology. **73**: 53–69. 1992.
5. Ivens IA, Loser E, Rinke M, Schmidt U, and Mohr U. Sunchronic toxicity of 2,3,7,8-tetrachlorodibenzo-*p*-dioxin in rats. Toxicology. **83**: 181–201. 1993.
6. Erin Staples E, Murante FG, Fiore NC, Gasiewicz TA, and Silverstone AE. Thymic alteration induced by 2,3,7,8-tetrachlorodibenzo-*p*-dioxin are strictly dependent on aryl hydrocarbon receptor activation in hemopoietic cells. J Immunol. **160**: 3844–3854. 1998.
7. Poland A and Knutson JC. 2,3,7,8-Tetrachlorodibenzo-*p*-dioxin and related halogenated aromatic hydrocarbons: examination of the mechanism of toxicity. Annu Rev Pharmacol Toxicol. **22**: 517–554. 1982.
8. Cook JC, Gaido KW, and Greenlee WF. Ah receptor: relevance of mechanistic studies to human risk assessment. Environ Health Perspect. **76**: 71–77. 1987.
9. Alsarif NZ, Lawson T, and Stohs SJ. Oxidative stress induced by 2,3,7,8-tetrachlorodibenzo-*p*-dioxin is mediated by the aryl hydrocarbon (Ah) receptor complex. Toxicology. **92**: 39–51. 1994a.
10. Stohs SJ, Hassan MQ, and Murray WJ. Lipid peroxidation as a possible cause of TCDD toxicity. Biochem Biophys Res Commun. **111**: 854–859. 1983.
11. Mohammadpour H, Murray WJ, and Stohs SJ. 2,3,7,8-Tetrachlorodibenzo-*p*-dioxin -induced lipid peroxidation in genetically responsive and non-responsive mice. Arch Environ Contam Toxicol. **17**: 645–650. 1988.
12. Wahba ZZ, Lawson TA, Murray WJ, and Stohs SJ. Factors influencing the induction of DNA single strand breaks in rats by 2,3,7,8-tetrachlorodibenzo-*p*-dioxin (TCDD). Toxicology. **58**: 57–69. 1989.
13. Al-Bayati ZAF, Murray WJ, and Stohs SJ. 2,3,7,8-Tetrachlorodibenzo-*p*-dioxin-induced lipid peroxidation in hepatic and extrahepatic tissues of male and female rats. Arch Environ Contam Toxicol. **16**: 159–166. 1987.
14. Alsharif NZ, Schlueter WJ, and Stohs SJ. Stimulation of NADPH-dependent reactive oxygen species formation and DNA damage by 2,3,7,8-tetrachlorodibenzo-*p*-dioxin in rat peritoneal lavage cells. Arch Environ Contam Toxicol. **26**: 392–397. 1994b.
15. Stohs SJ. Oxidative stress induced by 2,3,7,8-tetrachlorodibenzo-*p*-dioxin (TCDD). Free Radic Biol Med. **9**: 79–90. 1990.
16. Bondy SC and Naderi S. Contribution of hepatic cytochrome P450 systems to the generation of reactive oxygen species. Biochem Pharmacol. **48**: 155–159. 1994.
17. Floyd RA. Antioxidants, oxidative stress, and degenerative neurological disorders. Proc Soc Exp Biol Med. **222**: 236–245. 1999.
18. Hassoun EA, Li F, Abushaban A, and Stohs SJ. Production of superoxide anion, lipid oxidation and DNA damage in the hepatic and brain tissues of rats after subchronic exposure to mixtures of TCDD and its congeners. J Appl Toxicol. **21**: 211–219. 2001.
19. Tritscher AM, Seacat AM, Yager JD, Groopman JD, Miller BD, Bell D, Sutter TR, and Lucier GW. Increased oxidative DNA damage in livers of 2,3,7,8-tetrachlorodibenzo-*p*-dioxin treated intact but not ovarectomized rats. Cancer Lett.

98: 219–225. 1996.
20. Hassoun EA, Wilt SC, Devito MJ, Van Birgelen A, Alsharif NZ, Birnbaum LS, and Stohs SJ. Induction of oxidative stress in brain tissues of mice after subchronic exposure to 2,3,7,8-tetrachlorodibenzo-*p*-dioxin. Toxicol Sci. **42**: 23–27. 1998.
21. Slezak BP, Hatch GE, DeVito MJ, Diliberto JJ, Slade R, Crisman K, Hassoun E, and Birnbaum LS. Oxidative stress in female B6C3F1 mice following acute and subchronic exposure to 2,3,7,8-tetrachlorodibenzo-*p*-dioxin (TCDD). Toxicol Sci. **54**: 390–398. 2000.
22. Senft AP, Dalton TP, Nebert DW, Genter MB, Hutchinson RJ, and Shertzer HG. Dioxin increases reactive oxygen production in mouse liver mitochondria. Toxicol Appl Pharmacol. **178**: 15–21. 2002.
23. Nakamura H, Nakamura K, and Yodoi J. Redox regulation of cellular activation. Annu Rev Immunol. **15**: 351–369. 1997.
24. Nakamura H, Matsuda M, Furuke K, Kitaoka Y, Iwata S, Toda K, Inamoto T, Yamaoka Y, Ozawa K, and Yodoi J. Adult T cell leukemia-derived factor/human thioredoxin protects endothelial F-2 cell injury caused by activated neutrophils or hydrogen peroxide. Immunol Lett. **42**: 75–80. 1994.
25. Yokomise H, Fukuse T, Hirata T, Ohkubo K, Go T, Muro K, Yagi K, Inui K, Hitomi S, and Mitsui A. Effect of recombinant human adult T cell leukemia-derived factor on rat lung reperfusion injury. Respiration. **61**: 99–104. 1994.
26. Yoon BI, Hirabayashi Y, Kaneko T, Kodama Y, Kanno J, Yodoi J, Kim DY, and Inoue T. Transgene expression of thioredoxin (Trx/ADF) protects against 2,3,7,8-tetrachlorodibenzo-*p*-dioxin (TCDD)-induced hematotoxicity. Arch Environ Contam Toxicol. **41**: 232–236. 2001.
27. Takagi Y, Mitsui A, Nishiyama A, Nozaki K, Sono H, Gon Y, Hashimoto N, and Yodoi J. Overexpression of thioredoxin in transgenic mice attenuates focal ischemic brain damage. Proc Natl Acad Sci USA. **96**: 4131–4136. 1999.
28. Turner JN and Collins DN. Liver morphology in guinea pigs administered either pyrolysis products of a polychlorinated biphenyl transformer fluid or 2,3,7,8-tetrachlorodibenzo-*p*-dioxin. Toxicol Appl Pharmacol. **67**: 417–429. 1983.
29. Hassan MQ, Stohs SJ, and Murray WJ. Inhibition of TCDD-induced lipid peroxidation, glutathione peroxidase activity and toxicity by BHA and glutathione. Bull Environ Contam Toxicol. **34**: 787–796. 1985.
30. Hassan MQ, Stohs SJ, and Murray WJ. Effects of vitamin E and A on TCDD-induced lipid peroxidation and other biochemical changes. Arch Environ Contam Toxicol. **14**: 437–442. 1985.
31. Tanaka T, Nishiyama Y, Okada K, Hirota K, Matsui M, Yodoi J, Hiai H, and Toyokuni S. Induction and nuclear translocation of thioredoxin by oxidative damage in the mouse kidney: independence of tubular necrosis and sulfhydryl depletion. Lab Invest. **77**: 145–155. 1997.
32. Walker LJ, Robson CN, Black E, Gillespie D, and Hickson ID. Identification of residues in the human DNA repair enzyme HAP1 (Ref-1) that are essential for redox regulation of Jun DNA binding. Mol Cell Biol. **13**: 5370–5376. 1993.
33. Schenk H, Klein M, Erdbrügger W, Dröge W, and Schulze-Osthoff K. Distinct effects of thioredoxin and antioxidants on the activation of transcription factor NF-kB and AP-1. Proc Natl Acad Sci USA. **91**: 1672–1676. 1994.

Toxicologic Pathology, 32(Suppl. 2):12–16, 2004

ISSN: 0192-6233 print / 1533-1601 online
DOI: 10.1080/01926230490451725

Mechanism of Benzene-Induced Hematotoxicity and Leukemogenicity: Current Review with Implication of Microarray Analyses

YOKO HIRABAYASHI,[1] BYUNG-IL YOON,[1,2] GUANG-XUN LI,[1] JUN KANNO,[1] AND TOHRU INOUE[3]

[1]*Division of Cellular and Molecular Toxicology, National Institute of Health Sciences, Tokyo 158-8501, Japan*
[2]*Department of Veterinary Medicine, Kangwon National University, Kangwon 200-701, Republic of Korea, Seoul National University, Seoul 151-742, Republic of Korea, and*
[3]*Biological Safety and Research Center, National Institute of Health Sciences, Tokyo 158-8501, Japan*

ABSTRACT

Benzene is a potent human leukemogen but the mechanism underlying benzene-induced leukemia remains an enigma due to a number of questions regarding the requirement of extraordinarily long exposure, a relatively low incidence of leukemia for genotoxicity of metabolites and a narrow dose range for leukemogenicity over marrow aplasia (overdoses tend to result in marrow aplasia). Moreover, there were previous controversies as to whether the cell cycle is upregulated or suppressed by the benzene exposure. Subsequently, it was found that the cell cycle is suppressed, but how leukemia develops under such suppression of hemopoiesis remains to be clarified. These questions were fortunately resolved with much effort. Benzene exposure was found to induce the expression of p21, an interlocking counterdevice for cell cycle: due to *p53* upregulation, thereby inducing the immediate suppression of the kinetics of hemopoietic progenitors followed by the prominent suppression of hemopoiesis. Intermittent benzene exposure (i.e., cessation of exposure during weekends, for example) allowed an immediate recovery from marrow suppression after terminating exposure, which induced continuous oscillatory changes in marrow hemopoiesis. Benzene-induced leukemia was chiefly due to such an oscillatory change in hemopoiesis, which epigenetically developed leukemia more than 1 year later. The mechanisms of benzene-induced leukemogenicity seem to differ between wild-type mice and mice lacking *p53*. For *p53* knockout mice, DNA damage such as weak mutagenicity or chromosomal damage was retained, and such damage induced consequent activation of proto-oncogenes and related genes, which led cells to undergo further neoplastic changes. In contrast, for wild-type mice carrying the *p53* gene, a marked oscillatory change in the cell cycle of the stem cell compartment seems to be important. Compatible and discriminative gene expression profiling between the *p53* knockout mice and wild-type mice was observed after benzene exposure by microarray analyses.

Keywords. Benzene; hematotoxicity; leukemogenicity; gene chip array; BUUV method; *p53*-KO; AhR-KO; hemopoietic progenitor cells.

INTRODUCTION

The mechanism of benzene-induced leukemia had long been an enigma until recently, when the unique cell kinetics of stem/progenitor cells during benzene exposure was elucidated. Leukemia induction by benzene inhalation was first reported in 1897, when Le Noire described multiple cases of leukemia among Parisian cobblers (Le Noir and Claude, 1897). However, the experimental induction of leukemia by benzene exposure was first reported about 20 years ago by Snyder et al. (1980) and our group (Cronkite et al., 1984, 1989). Recently, we demonstrated marked oscillatory changes in peripheral blood and bone marrow (BM)[1] cellularities during and following benzene inhalation, preceding the development of leukemia by about 1 year (Hirabayashi et al., 1998; Kawasaki et al., 2001; Yoon et al., 2001).

Benzene-induced leukemia is unique in that it has been associated only with a weak mutagenicity in the benzene metabolites, phenol and hydroquinone. Another interesting observation is the controversial experimental data concerning the level of actively cycling hematopoietic cells following benzene exposure. While all researchers observed a decrease in peripheral blood and BM cellularities, some observed a suppression of the cell cycle of BM, as measured by tritiated thymidine incorporation (Moeschlin and Speck, 1967), whereas others observed a marked increase in the number of cycling stem/progenitor cells in BM and peripheral blood (Table 1). Careful analysis of these apparently conflicting data revealed an enhancement of the cell cycle occurring at least 2 hours after the termination of benzene exposure. Thus, the higher tritiated thymidine incorporation documented by Cronkite et al. (1982) 18 hours after the termination of benzene exposure probably reflects a recovery phase. Based on these findings, we conducted a series of studies since 1997 to elucidate the leukemogenic effect of benzene in wild-type mice.

The *p53*-knockout (KO) mouse (Tsukada et al., 1993) showed further unique characteristics of benzene-induced leukemia. Using *p53*-KO mouse, we confirmed that benzene has a moderate genotoxic effect, as measured by the micronucleus test performed 4 weeks after the initiation of benzene inhalation (Kawasaki et al., 2001; Li et al., 2003). Moreover, *p53*-deficient mice manifest increased susceptibility to

Address correspondence to: Tohru Inoue, Center for Biological Safety and Research, National Institute of Health Sciences, 1-18-1 Kamiyohga, Setagayaku, Tokyo 158-8501, Japan; e-mail: tohru@nihs.go.jp

[1]Abbreviations: BM, bone marrow; KO, knockout; UV, ultraviolet; BUUV, incorporation of bromodeoxyuridine followed by ultraviolet-light cytocide to evaluate the hemopoietic stem/progenitor cell kinetics in vivo; AhR, aryl hydrocarbon receptor; $AhR^{+/+}$, AhR wild-type; $AhR^{+/-}$, AhR heterozygous-deficient; $AhR^{-/-}$, AhR homozygous-deficient; CFU-GM, granulo-macrophage colony forming unit; CYP, cytochrome P450; FGF, fibroblast growth factor; TGF, tumor growth factor; I.V., intravenous; I.P., intraperitoneal; aft, after; dur, during; expos, exposure.

TABLE 1.—Summary of the results the hemopoietic stem/progenitor cell kinetics during and after benzene exposure by tritiated thymidine (^{3}H-TdR) cytocide assay.

				Evaluation cell and assay methods					
		Cellularity		BM cells			CFU		
Year	Reference	Blood	BM	Kinetics	Labeling*,1	Label point	Kinetics	Labeling	Label point
1967	Moeschlin and Speck	↓	↓	↓	In vivo	At pancytopenia	—	—	—
1979	Irons et al.	↓	↓	↑	In vivo[2]	6 days aft. expos-IP	—	—	—
1982	Cronkite et al.	↓	↓	—	—	—	↑	In vitro	18 h aft. expos.
1998	Lee et al.	↓	↓	↓	In vivo[3]	30 min aft. single IP	—	—	—
		↓	↓	↓	In vitro	Dur. and aft. expos.	—	—	—
1997	Farris et al.	↓	↓	→↓	In vivo[4]	Soon aft. expos.	↑	In vitro	2 h aft. expos.

1. ^{3}H-TdR was injected intravenous (IV) at in vivo labeling except indications.
2. ^{3}H-TdR was injected intraperitoneal (IP) 6 days after cessation of benzene.
3. Benzene was treated single IP, and ^{3}H-TdR label was starting 30 minutes after benzene treatment.
4. Instead of ^{3}H-TdR, BrdUrd was used for assay.

benzene-induced leukemogenicity (Kawasaki et al., 2001). Similar findings with regard to increased leukemogenicity following benzene exposure have been documented by French et al. of the National Institute of Environmental Health Sciences (French et al., 2001). Contrary to the result in *p53*-KO mice, benzene-induced leukemia had not been detected in earlier studies in wild-type mice because its manifestations had been masked either by pancytopenia due to severe myelosuppression or by the use of a benzene dose too low to induce pancytopenia or leukemia (Kawasaki et al., 2001). Aryl hydrocarbon receptor (AhR)-KO mice (Mimura et al., 1997) also elucidated the characteristic underlying mechanism of benzene-induced hematotoxicity (Yoon et al., 2002).

In the mechanism underlying benzene toxicity in BM tissue analyzed using a microarray system, various signaling pathways have been suggested to be implicated including cell cycle regulation, DNA-damage/repair-related genes, oxidative-stress-related genes, growth-factor-related genes, oncogenes, and hemopoiesis-related genes in general (Yoon et al., 2003).

OSCILLATORY CHANGES IN BONE MARROW CELLULARITY IN WILD-TYPE MICE

BM cellularity decreases markedly during benzene inhalation but recovers rapidly following the termination of benzene exposure (Yoon et al., 2001). The oscillatory nature of the resultant curve is comparable to the response reported by Cronkite et al. (1984, 1989), and suggests that benzene does not only induce BM cell suppression but also activates cell-cycle-regulating genes, resulting in compensatory myelopoiesis.

We used the BUUV (bromodeoxyuridine + UV exposure) method to study stem/progenitor cell kinetics during or after benzene exposure (Hirabayashi et al., 1998; Yoon et al., 2001). Using this method, we were able to measure the labeling rate, cycling fraction of clonogenic progenitor cells, and other cell cycle parameters. Interestingly, the cycling fraction of stem/progenitor cells was found not to turn into active hematopoiesis but to remain low during benzene inhalation. Furthermore, rapid recovery was observed after benzene inhalation was terminated (Figure 1). However, although the exact mechanism of this phenomenon is not yet known, we found the evidence that the cycling fraction depression may be mediated in part by the suppression of stem/progenitor cell cycling per se, owing to the *p53*-dependent upregulation of p21 (Yoon et al., 2001). Thus, the mechanism of benzene-induced leukemia in the wild-type mice may be due to continuous oscillatory changes in hemopoiesis during and after the benzene exposure, which leads to genetic instability followed by the consequent epigenetic leukemogenicity.

p53-DEFICIENT MICE DEVELOP LEUKEMIA BY DIFFERENT MECHANISMS

Leukemogenicity induced in *p53*-KO mice, because of the lack of the *p53* gene, results in the noninduction of p21 expression even during the benzene exposure, with subsequent insufficient DNA repair and accumulation of DNA damage. These pathways are shown in Figure 2 for benzene-induced possible toxicological changes in both wild-type and *p53*-KO mice. In *p53*-KO mice, cell cycle suppression, DNA repair, and apoptosis of damaged cells, which, in general, occur in the wild-type mice after benzene exposure, are all suppressed. This is much more likely genotoxic leukemogenesis, in which reactive oxygen species, dysfunction of topoisomerase, and covalent binding of adduct formation to DNA,

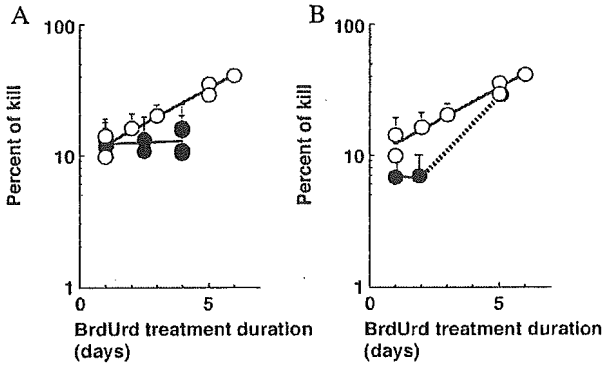

FIGURE 1.—Hemopoietic progenitor cell (CFU-GM) kinetics during (A) and after (B) benzene inhalation. Open circle: sham; Closed circle: during or after inhalation of 300 ppm benzene, 6 h/day, 5 days/week ×2 weeks. (A) For the benzene-treated group, all the mice were sacrificed just after the 5th day of the 2nd week of benzene-inhalation. The osmotic minipump filled with BrdUrd was implanted into donor mice day(s) before sacrificing as indicated on the abscissa. (B) For the benzene-treated group, the BrdUrd-pump was implanted into donor mice after the 5th day of the 2nd week of benzene-inhalation and sacrificed on the day as indicated on the abscissa. Each point represents at least 2 mice as a donor for the CFU-GM assay, and colony assays were performed in triplicate.

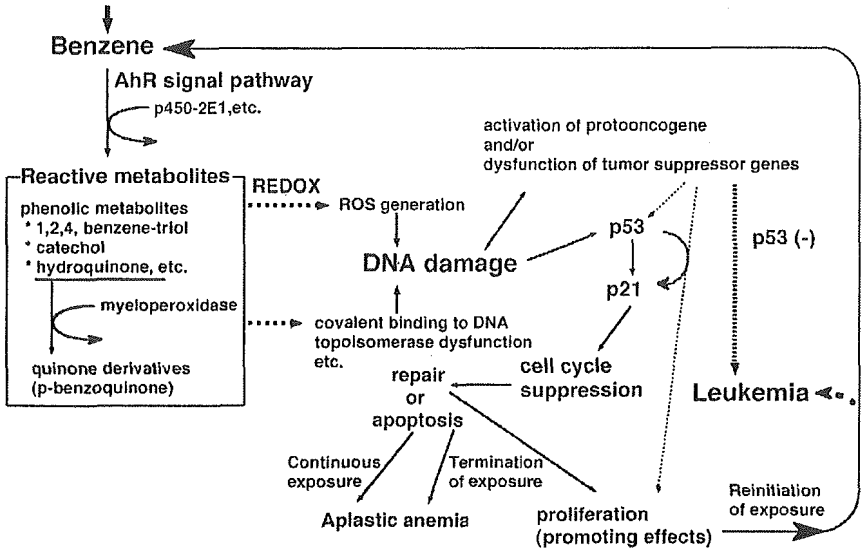

FIGURE 2.—Benzene metabolism and possible mechanism of benzene-induced leukemogenesis.

all synergistically participate in further leukemogenic development without repairing the system (see Figure 2). Thus, leukemogenicity seems to be clearly different between the mice carrying wild-type *p53* and the mice lacking *p53* (Yoon et al., 2001; Hirabayashi et al., 2002).

ARYLHYDROCARBON-RECEPTOR-MEDIATED BENZENE METABOLISM

We investigated the involvement of the aryl hydrocarbon receptor (AhR), a ligand-activated basic helix-loop-helix transcription factor, in hematotoxicity using AhR wild-type ($AhR^{+/+}$), heterozygous-KO ($AhR^{+/-}$) and homozygous-KO ($AhR^{-/-}$) male mice (Mimura et al., 1997; Yoon et al., 2002). Following a 2-week inhalation of benzene at 300 ppm, we evaluated the changes in cellularity of the peripheral blood and BM, and the levels of granulocyte-macrophage colony-forming units (CFU-GM) in the BM (Figure 3). The expression of the cyclin-dependent kinase inhibitor, p21, in BM cells and cytochrome P450 (CYP) 2E1 in hepatic tissues were evaluated by Western blot analysis after benzene exposure. Our results clearly showed that $AhR^{-/-}$ mice are much more resistant to the benzene-induced hematotoxicity than $AhR^{+/+}$ wild-type mice. No changes in p21 expression level by BM cells were detected in $AhR^{-/-}$ mice, whereas a marked up-regulation of p21 expression by BM cells was observed in $AhR^{+/+}$ mice. This finding is a further proof of the resistance of $AhR^{-/-}$ mice to benzene-induced hematotoxicity. The benzene resistance of $AhR^{-/-}$ mice was abrogated by exposure to a combination of 2 major metabolites, phenol and hydroquinone, strongly supporting the notion that AhR participates in benzene metabolism. CYP species involved in such metabolism are under investigation. The results obtained imply that pollutants that react with AhR confer marked susceptibility to benzene-induced hematotoxicity.

IMPLICATION OF MICROARRAY ANALYSIS

In the mechanism underlying benzene toxicity in BM tissue, various signaling pathways have been suggested to be implicated including metabolism, genotoxicity, cell cycle regulation, and apoptosis (Table 2). Our microarray analysis

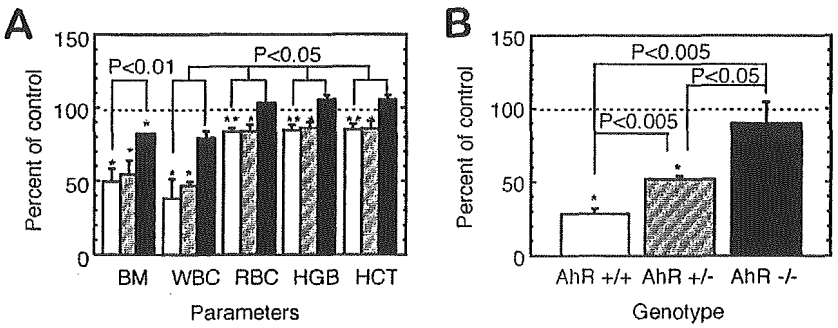

FIGURE 3.—Changes in peripheral blood parameters and BM cellularity (A) and CFU-GM per 2 femurs (B) in the AhR wild-type ($AhR^{+/+}$:open bar), heterozygous-KO ($AhR^{+/-}$:shaded bar) and homozygous-KO mice ($AhR^{-/-}$:closed bar) exposed to 300 ppm benzene for 2 weeks. The mean BM cellularities for the $AhR^{+/+}$, $AhR^{+/-}$, and $AhR^{-/-}$ mice were 4.8, 5.6, and 4.8 $\times$ 10^7/2 femurs, respectively, and the mean numbers of CFU-GM's per 8 $\times$ 10^4 BM cells was 79, 78, and 72, respectively. *, **: Significantly different from each corresponding control group at $p < 0.05$ and $p < 0.01$, respectively.

TABLE 2.—Reported genes whose expression changed during and/or after benzene inhalation.

Category	Gene name	Reference
Metabolic enzyme	CYP 2E1	Zhang et al., 2002
	Myeloperoxidase	Schattenberg et al., 1994
Cell cycle	*p53*	Boley et al., 2002
	p21 (waf 1)	
	Cyclin G	
	Gadd 45	
Apoptosis	Bax-alpha	Boley et al., 2002
Oncogene	c-fos	Ho and Witz, 1997

elucidated the up- or downregulation of genes functioning after 2-week exposure to 300 ppm benzene (Table 3): First, among cell-cycle-related genes, in addition to *p53* and p21 which are known to be upregulated to various extents depending upon the time course and the detection methods, Rb-related genes, such as the Rb-related protein p130 and the Rb-binding protein p48 are significantly upregulated; furthermore, elongation factor 1-delta shows a high expression level associated with the G2/M cell cycle checkpoint; vice versa, a significant downregulation of cyclin D1 and BimB is also recognized. Less significant changes in expression of cyclin G and Gadd45 are noted as previously reported. Second, among DNA-damage/repair-related genes, those encoding ADP-ribosylation factor-like protein 1 and Rad51 are significantly upregulated. The altered expression of other genes in the same category such as Metaxin, ERCC-3, and the DTR111 precursor are also noted, although p-values are not statistically significant. Third, among oxidative-stress-related genes, mitogen-activated protein kinase 2, which responds primarily to stress and inflammatory stimuli, is significantly upregulated, and the known typical ROS absorber genes, such as those encoding GST-1 and UDP glucuronosyltransferase show mild but significant increases. C3h-dioxin-inducible cytosolic aldehyde dehydrogenase-3, Cytochrome c oxidase Vb, and lactate dehydrogenase are also upregulated. Fourth, among growth-factor-related genes, those encoding the hepatocyte-growth factor-like protein shows significant upregulation, associated with a slight increase/decrease in expression level, with less significant p-values, for the following genes: fibroblast growth factor (FGF)-15, FGF-b, G protein-coupled receptor, growth factor-induced delayed-early-response protein, insulin-like growth factor 1 receptor precursor, insulin-induced growth response protein cl-6, tumor growth factor (TGF)-beta 1, TGF-beta 1 masking protein, and tumor necrosis factor alpha. Fifth, among the gene expression profiling of oncogenes, RhoB, which is possibly related to the genotoxic effect of benzene metabolites, shows a high expression level. Finally, hemopoiesis-related genes also show particular changes in their expression level, but the profiling of such genes led to the elucidation that benzene generally induces suppression of cell proliferation without an increase in cytokine gene expression levels.

It is of interest to determine gene expression in *p53*-KO mice with or without exposure by benzene inhalation (Yoon et al., 2003). In Table 3, the annotated genes were all downregulated (top) or upregulated (bottom) after benzene exposure, although their expressions were not altered in the wild-type mice, implying that the expressions of these genes are masked by the homeostasis governed by *p53* gene regulation. Thus, this study on *p53*-KO mice led to the elucidation of hidden gene alterations in wild-type mice, which we do not generally observe in toxicological examination.

TABLE 3.—*p53*-related genes whose expression level decreased or increased by benzene exposure, but unchanged in the wild-type mice.

WT: unchanged *p53*-KO: decreased	CalDAG-GEFI, Cbfa2, Dctn1, Frl, Grl-1, Ig/EBP, Klra3, Mek5, MEP, Mlp1, B-myb, Nog, PBX2, Prkm3, PTPalpha, Rad50, Rad51, Zfp94
WT: unchanged *p53*-KO: increased	24p3, 4E-BP2, Abcg2, ACRP, Activine, Ahd3, Alp, Anx3, AOE372, Apaf1, BAG-1, BAP, bcl-2, Calcyclin, Canexin, Caspase 9, Caspase 9S, CCR1, CD3 theta, CD71, CD143, Cox5b, Cox7a1, COX8H, Ctla-2a, Cu/Zn-SOD, Cyclin B1, DCIR, Dnmt2, Dpagt2, E4BP4, EPO, FACS, Fes, elk1, G6PD, G6PD-2, Galbp, Gapdh, Gcdh, Gdi2, Growth hormone, Gnb-1, Gng3lg, H-2T18, HES-1, IGF-1, IL1bc, IL-4, IL-9, JSR1, LDH-1, LDH-2, mLigI, Lipo 1, Lrf, Ly-3, Ly-40, Jam, JNK2, Kcc1, KSR1, M-CSF, Mac-1 alpha, Mch6, Mg11, MHR23A, MmCEN3, Mrad17, MRP14, Mtx2, NFATp, NL, Nmo1, OERK, PAFR, Pde8, PERK, PGRP, Pla2g2c, PLGF, Pop2, Prkm9, Prtn3, RBP-L, Rga, S100A13, Siva, Smad 6, SPRR2J, Stat4, Stat 5B, TCF4, TOM1, Trypsin 2, Tst

See reference, Yoon et al. (2003).

REFERENCES

Boley, S. E., Wong, V. A., French, J. E., and Recio, L. (2002). *p53* heterozygosity alters the mRNA expression of *p53* target genes in the bone marrow in response to inhaled benzene. *Toxicol Sci* **66**, 209–15.

Cronkite, E. P., Bullis, J., Inoue, T., and Drew, R. T. (1984). Benzene inhalation produces leukemia in mice. *Toxicol Appl Pharmacol* **75**, 358–61.

Cronkite, E. P., Drew, R. T., Inoue, T., Hirabayashi, Y., and Bullis, E. (1989). Hematotoxicity and carcinogenicity of inhaled benzene. *Environ Health Perspect* **82**, 97–108.

Cronkite, E. P., Inoue, T., Carsten, A. L., Miller, M. E., Bullis, J. E., and Drew, R. T. (1982). Effects of benzene inhalation on murine pluripotent stem cells. *J Toxicol Environ Health* **9**, 411–21.

Farris, G. M., Robinson, S. N., Gaido, K. W., Wong, B. A., Wong, V. A., Hahn, W. P., and Shah, R. S. (1997). Benzene-induced hematotoxicity and bone marrow compensation in B6C3F1 mice. *Fundam Appl Toxicol* **36**, 119–29.

French, J. E., Lacks, G. D., Trempus, C., Dunnick, J. K., Foley, J., Mahler, J., Tice, R. R., and Tennant, R. W. (2001). Loss of heterozygosity frequency at the *Trp53* locus in *p53*-deficient (+/−) mouse tumors is carcinogen- and tissue-dependent. *Carcinogenesis* **22**, 99–106.

Hirabayashi, Y., Matsumura, T., Matsuda, M., Kuramoto, K., Motoyoshi, K., Yoshida, K., Sasaki, H., and Inoue, T. (1998). Cell kinetics of hemopoietic colony-forming units in spleen (CFU-S) in young and old mice. *Mech Ageing Dev* **101**, 221–31.

Hirabayashi, Y., Yoon, B. I., Kawasaki, Y., Li, G. X., Kanno, J., and Inoue, T. (2002). On the mechanistic differences of benzene-induced leukemogenesis between wild type and *p53* knockout mice. *Molecular Mechanisms for Radiation-Induced Cellular Response and Cancer Development* (K. Tanaka, T. Takabatake, K. Fujikawa, T. Matsumoto, and F. Sado, eds.), pp. 110–16. Aomori, Institute for Environmental Sciences, Japan.

Ho, T. Y., and Witz, G. (1997). Increased gene expression in human promyeloid leukemia cells exposed to trans, trans-muconaldehyde, a hematotoxic benzene metabolite. *Carcinogenesis* **18**, 739–44.

Irons, R. D., Heck, H., Moore, B. J., and Muirhead, K. A. (1979). Effects of short-term benzene administration on bone marrow cell cycle kinetics in the rat. *Toxicol Appl Pharmacol* **51**, 399–409.

Kawasaki, Y., Hirabayashi, Y., Yoon, B. I., Huo, Y., Kaneko, T., Kurokawa, Y., and Inoue, T. (2001). Benzene inhalation induced an early onset and a high incidence of leukemias in the *p53* deficient C57BL/6 mice. *Jpn J Cancer Res* **92**(Suppl), 71.

Lee, E. W., Garner, C. D., and Johnson, J. T. (1988). A proposed role played by benzene itself in the induction of acute cytopenia: inhibition of DNA synthesis. *Res Commun Chem Pathol Pharmacol* **60**, 27–46.

Le Noir and Claude (1897). Sur un cas de purpura atribué a l'intoxication par la benzine. *Bull Med Soc Hop Paris* **14**, 1251–60.

Li, G. X., Hirabayashi, Y., Yoon, B. I., Kawasaki, Y., Kurokawa, Y., Yodoi, J., Kanno, J., and Inoue, T. (2003). Benzene-induced leukemia is prevented by over-expression of Trx/ADF, along with increase in Trx/ADF-expression, increase in SOD-activity, and decrease in micronuclei. *Cancer Science* **94**(suppl), 265.

Mimura, J., Yamashita, K., Nakamura, K., Morita, M., Takagi, T. N., Nakao, K., Ema, M., Sogawa, K., Yasuda, M., Katsuki, M., and Fujii-Kuriyama, Y. (1997). Loss of teratogenic response to 2,3,7,8-tetrachlorodibenzo-*p*-dioxin (TCDD) in mice lacking the Ah (dioxin) receptor. *Genes Cells* **2**, 645–54.

Moeschlin, S., and Speck, B. (1967). Experimental studies on the mechanism of action of benzene on the bone marrow (radioautographic studies using 3H-thymidine). *Acta Haematol* **38**, 104–11.

Schattenberg, D. G., Stillman, W. S., Gruntmeir, J. J., Helm, K. M., Irons, R. D., and Ross, D. (1994). Peroxidase activity in murine and human hematopoietic progenitor cells: potential relevance to benzene-induced toxicity. *Mol Pharmacol* **46**, 346–51.

Snyder, C. A., Goldstein, B. D., Sellakumar, A. R., Bromberg, I., Laskin, S., and Albert, R. E. (1980). The inhalation toxicology of benzene: incidence of hematopoietic neoplasms and hematotoxicity in ARK/J and C57BL/6J mice. *Toxicol Appl Pharmacol* **54**, 323–31.

Tsukada, T., Tomooka, Y., Takai, S., Ueda, Y., Nishikawa, S., Yagi, T., Tokunaga, T., Takeda, N., Suda, Y., Abe, S., Matsuo, I., Ikawa, Y., and Aizawa, S. (1993). Enhanced proliferative potential in culture of cells from *p53*-deficient mice. *Oncogene* **8**, 3313–22.

Yoon, B. I., Hirabayashi, Y., Kawasaki, Y., Kodama, Y., Kaneko, T., Kim, D. Y., and Inoue, T. (2001). Mechanism of action of benzene toxicity: cell cycle suppression in hemopoietic progenitor cells (CFU-GM). *Exp Hematol* **29**, 278–85.

Yoon, B. I., Hirabayashi, Y., Kawasaki, Y., Kodama, Y., Kaneko, T., Kanno, J., Kim, D. Y., Fujii-Kuriyama, Y., and Inoue, T. (2002). Aryl hydrocarbon receptor mediates benzene-induced hematotoxicity. *Toxicol Sci* **70**, 150–6.

Yoon, B. I., Li, G. X., Kitada, K., Kawasaki, Y., Igarashi, K., Kodama, Y., Inoue, T., Kobayashi, K., Kanno, J., Kim, D. Y., and Hirabayashi, Y. (2003). Mechanisms of benzene-induced hematotoxicity and leukemogenicity: cDNA microarray analyses using mouse bone marrow tissue. *Environ Health Perspect* **111**, 1411–20.

Zhang, S., Cawley, G. F., Eyer, C. S., and Backes, W. L. (2002). Altered ethylbenzene-mediated hepatic CYP2E1 expression in growth hormone-deficient dwarf rats. *Toxicol Appl Pharmacol* **179**, 74–82.

ehp Environmental Health
ehponline.org
PERSPECTIVES
Journal of the National Institute of Environmental Health Sciences

Reprinted from:

August 2003
VOLUME 111 | NUMBER 11

The National Institute of Environmental Health Sciences
National Institutes of Health
U.S. Department of Health and Human Services

Toxicogenomics

Mechanisms of Benzene-Induced Hematotoxicity and Leukemogenicity: cDNA Microarray Analyses Using Mouse Bone Marrow Tissue

Byung-IL Yoon,[1] Guang-Xun Li,[1] Kunio Kitada,[2] Yasushi Kawasaki,[1] Katsuhide Igarashi,[1] Yukio Kodama,[1] Tomoaki Inoue,[2] Kazuko Kobayashi,[2] Jun Kanno,[1] Dae-Yong Kim,[3] Tohru Inoue,[4] and Yoko Hirabayashi[1]

[1]Division of Cellular and Molecular Toxicology, National Institute of Health Sciences, Tokyo, Japan; [2]Kamakura Research Labs, Chugai Pharmaceutical, Co., Ltd., Kamakura, Japan; [3]Department of Veterinary Pathology, College of Veterinary Medicine and Agricultural Biotechnology, Seoul National University, Seoul, Republic of Korea; [4]Biological Safety and Research Center, National Institute of Health Sciences, Tokyo, Japan

Although the mechanisms underlying benzene-induced toxicity and leukemogenicity are not yet fully understood, they are likely to be complicated by various pathways, including those of metabolism, growth factor regulation, oxidative stress, DNA damage, cell cycle regulation, and programmed cell death. With this as a background, we performed cDNA microarray analyses on mouse bone marrow tissue during and after a 2-week benzene exposure by inhalation. Our goal was to clarify the mechanisms underlying the hematotoxicity and leukemogenicity induced by benzene at the level of altered multigene expression. Because a few researchers have postulated that the cell cycle regulation mediated by p53 is a critical event for benzene-induced hematotoxicity, the present study was carried out using p53-knockout (KO) mice and C57BL/6 mice. On the basis of the results of large-scale gene expression studies, we conclude the following: *a)* Benzene induces DNA damage in cells at any phase of the cell cycle through myeloperoxidase and in the redox cycle, resulting in *p53* expression through *Raf-1* and cyclin D-interacting myb-like protein 1. *b)* For G1/S cell cycle arrest, the p53-mediated pathway through p21 is involved, as well as the pRb gene–mediated pathway. *c)* Alteration of *cyclin G1* and *Wee-1 kinase* genes may be related to the G2/M arrest induced by benzene exposure. *d)* DNA repair genes such as *Rad50* and *Rad51* are markedly downregulated in p53-KO mice. *e)* p53-mediated caspase 11 activation, aside from p53-mediated *Bax* gene induction, may be an important pathway for cellular apoptosis after benzene exposure. Our results strongly suggest that the dysfunction of the *p53* gene, possibly caused by strong and repeated genetic and epigenetic effects of benzene on candidate leukemia cells, may induce fatal problems such as those of cell cycle checkpoint, apoptosis, and the DNA repair system, finally resulting in hemopoietic malignancies. Our cDNA microarray data provide valuable information for future investigations of the mechanisms underlying the toxicity and leukemogenicity of benzene. *Key words:* apoptosis, benzene, cDNA microarray, cell cycle, DNA damage, DNA repair, hematotoxicity, leukemia, oxidative stress, p53-knockout mice. *Environ Health Perspect* 111:1411–1420 (2003). doi:10.1289/txg.6164 available via *http://dx.doi.org/* [Online 5 August 2003]

Benzene is well documented as an environmental pollutant that can induce hematotoxicity and hemopoietic neoplasia in humans and mice (Aksoy et al. 1974, 1976; Cronkite et al. 1984, 1989; Snyder et al. 1980; Vigliani and Forni 1976). To date, studies on benzene have focused on its metabolic pathways to determine the metabolites responsible for its hematotoxicity and leukemogenicity (Henderson 1996; Schlosser et al. 1989; Schrenk et al. 1996; Snyder and Hedli 1996). Benzene and its major metabolites are not mutagenic in the Ames *Salmonella* test (Dean 1985), but they do induce chromosomal aberration both *in vitro* and *in vivo* (Dean 1985; Wolman 1977; Yager et al. 1990). This is comparable to classic carcinogens that are generally being activated to a single carcinogenic metabolite having a mutagenic property. Benzene can be characterized further in terms of its multisite carcinogenicity (Huff et al. 1989; Maltoni et al. 1989). Mice exposed to benzene develop different types of tumor in various glandular tissues and organs, including the hemopoietic system, Zymbal gland, Harderian gland, preputial gland, mammary gland, ovary, and lung. Results of the study of Low et al. (1995) strongly suggest that the carcinogenicity of benzene on target organs depends on the ability of enzymes in the organs to metabolize benzene.

As postulated by several investigators, the metabolism of benzene to reactive metabolites by hepatic enzymes, mainly cytochrome P450-2E1 (CYP2E1), is a prerequisite to the cyto- and genotoxicities associated with benzene exposure (Gut et al. 1996; Snyder and Hedli 1996; Valentine et al. 1996). Primary benzene metabolites include phenol, hydroquinone, catechol, and *trans-trans* muconic acid (Ross 2000). The synergistic interactions between these phenolic metabolites exacerbate benzene toxicity (Chen and Eastmond 1995; Eastmond et al. 1987; Subrahmanyam et al. 1990). This mechanism of multimetabolite genotoxicity is another unique aspect of benzene that distinguishes it from other chemicals in terms of the mechanism of its toxicity and carcinogenicity. Benzene metabolites subsequently undergo secondary activation by myeloperoxidase (MPO) that is present at high levels in the bone marrow tissue. This results in the production of genotoxic quinones and reactive oxygen species, thereby inducing not only hemopoietic cellular damage (Farris et al. 1997; Kolachana et al. 1993; Lee and Garner 1991; Smith et al. 1989) but also the dysfunction of bone marrow stromal cells (Niculescu et al. 1995).

Exposure duration and dose are also important factors in determining benzene-induced hematotoxicity and leukemogenicity (Cronkite et al. 1989; Snyder and Kalf 1994), which may be related to the limited capacity of enzymes for benzene metabolism and to the dynamic responses of hemopoietic microenvironmental conditions against the adverse effects of benzene.

Despite intensive studies over several decades, the mechanisms underlying benzene-induced hematotoxicity and leukemogenicity are still not fully understood. Nevertheless, previous studies strongly suggest that the toxic effects of benzene on bone marrow tissue can be realized through pathways such as those of metabolism (Snyder and Hedli 1996), growth factor regulation (Niculescu et al. 1995),

Address correspondence to Y. Hirabayashi, Division of Cellular and Molecular Toxicology, Biological Safety and Research Center, National Institute of Health Sciences, 1-18-1 Kamiyoga, Setagayaku, Tokyo 158-8501 Japan. Telephone: 81 3 3700 9639. Fax: 81 3 3700 9647. E-mail: yokohira@nihs.go.jp

We thank E. Tachihara, Y. Usami, and Y. Shinzawa for their excellent technical assistance and N. Katsu and Y. Nagano for their help in manuscript preparation. We also thank the late E. Cronkite for constructive discussion and comments on the manuscript.

This work was supported by the Japan Health Sciences Foundation (research on health sciences focusing on drug innovation, KH31034).

The authors declare they have no conflict of interest.

Received 17 December 2002; accepted 10 July 2003.

production of oxidative stress (Laskin et al. 1996; Subrahmanyam et al. 1991), DNA damage and repair (Lee and Garner 1991), cell cycle regulation (Yoon et al. 2001b), and apoptosis (Moran et al. 1996; Ross et al. 1996). These studies indicate that investigation of the roles of a few specific genes may not be sufficient to explain the complete molecular mechanism of benzene-induced hematotoxicity and leukemogenicity.

Bone marrow tissue, a major target organ of benzene, is an active hemopoietic system in which various counterbalanced genes are organized through their network interactions that maintain cellular–environmental homeostasis as well as protect cells from endogenous and exogenous hematotoxic effects such as benzene-induced effects. The dysregulation of such a multidimensional counterbalance, possibly induced by the genetic and epigenetic effects of benzene, may result in the altered expression of a number of genes associated with the mechanisms of benzene-induced hematotoxicity and leukemogenicity.

In this study we investigated the changes in DNA expression during and after benzene exposure (300 ppm) to probe further the molecular mechanisms underlying benzene toxicity. Because previous studies (Boley et al. 2002; Yoon et al. 2001b) demonstrated that the *p53* tumor suppressor gene is important in cell cycle regulation associated with the mechanisms of benzene-induced toxicity, these analyses were carried out by cDNA microarray analyses in C57BL/6, wild-type (WT), and p53-knockout (KO) mice.

Materials and Methods

Animals

Specific pathogen–free, 7-week-old, male C57BL/6 mice were purchased from Japan SLC (Hamamatsu, Japan) and quarantined for 1 week in 1.3-m^3 inhalation chambers (Shibata Scientific Technology Ltd., Tokyo, Japan) in ambient air. To obtain WT and p53-KO mice for use in this study, male and female heterozygous p53-KO C57BL/6 mice, originally bioengineered by Tsukada et al. (1993), were mated; the pups produced were then identified by polymerase chain reaction analysis of the DNA samples extracted from the tail of each mouse. The mice were grouped randomly into untreated control and benzene-exposed groups and maintained in stainless-steel wire cages inside inhalation chambers under a 12-hr light–dark cycle during the study. A basic pellet diet (CRF-1; Funabashi Farm, Funabashi, Japan) was provided *ad libitum* except during the daily 6-hr benzene inhalation period. Water was delivered by an automated tubing nozzle and provided *ad libitum* throughout the study.

Benzene Exposure

Benzene vapor was generated and its concentration was monitored as described elsewhere (Yoon et al. 2001b). Temperature and humidity inside the chambers were maintained automatically at 24 ± 1°C and 55 ± 10%, respectively. Mice were exposed to 300 ppm benzene for 6 hr/day, 5 days/week for 2 weeks; the sham control groups were maintained in the inhalation chambers in ambient air over the same period. Experimental schedules for sham and benzene-treated mice are shown in Figure 1. Immediately after the first 5 days of exposure (D5), the second 5 days of exposure in the second week (D12), and 3 days after D12 for recovery (D+3), the mice were sacrificed. D12 is also designated as the 2-week exposure. To investigate changes in gene expression, three C57BL/6 mice from each of the sham control and benzene-exposed groups were decapitated after euthanasia at 1 week (D5) and 2 weeks (D12), respectively, during a 2-week benzene exposure period and 3 days after benzene removal (D+3), and poly(A)$^+$ RNA extracted from each group was applied to Incyte gene expression microarray (GEM) assay (Incyte Pharmaceuticals, Inc., Palo Alto, CA, USA) (see "Microarray Preparation"). Our previous study (Yoon et al. 2001b) showed that mice are able to recover from benzene-induced hematotoxicity 3 days after a 2-week benzene exposure. In studies using WT and p53-KO mice, two to four mice from each group and genotype were sacrificed immediately after the 2-week benzene exposure and applied to the Affymetrix system (Affymetrix, Inc., Santa Clara, CA, USA) (see "Microarray Preparation").

Bone Marrow Cell Collection for RNA Extraction

The mice from which bone marrow cells were collected for RNA extraction were carefully chosen on the basis of our evaluation of peripheral blood number and bone marrow cellularity using a blood cell counter (Sysmex M-2000; Sysmex Co., Tokyo, Japan) and our comparison of the values with those previously reported (Yoon et al. 2001b).

We harvested bone marrow cells from both femurs of individual mice of each group (Yoon et al. 2001b). Using a 27-gauge hypodermic needle, we flushed out bone marrow cells of the bone shafts with 2 mL Dulbecco's modified minimum essential medium without phenol red (Invitrogen Corp., Carlsbad, CA, USA). Single-cell suspensions were then prepared by repeatedly passing the harvested bone marrow cells through the needle. After the lysis of red blood cells, the bone marrow cells were immediately frozen in liquid nitrogen and stored at –80°C until RNA extraction.

Preparation of Total RNA and Poly(A)$^+$ RNA

Total RNA was extracted from the collected bone marrow cells using ISOGEN (Wako Chemical Co., Osaka, Japan) in accordance with the manufacturer's instructions. The total RNA yielded optical density (OD) ratios (OD 260/280) of 1.7–2.1; its purity was confirmed by gel

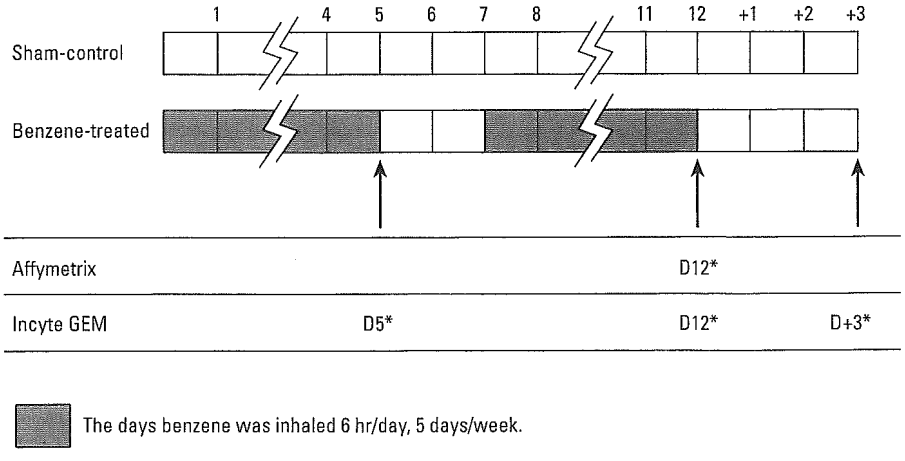

Figure 1. Benzene inhalation schedule diagram: exposure was for 6 hr/day from 10 A.M. to 4 P.M. On the days marked with an asterisk (*), both sham exposure mice were killed at 4 P.M., and exposed mice were killed immediately after exposure (Yoon et al. 2002). On D+3, both sham and recovery mice were killed at 4 P.M. D5 designates practically a 1-week exposure and D12, a 2-week exposure. D+3 is the group with a 3-day recovery period after D12.

chromatography, and its concentration was determined on the basis of its absorbance at 260 nm that was measured with a Beckman spectrophotometer (DU640; Beckman Coulter, Inc., Fullerton, CA, USA). Independent total RNA and poly(A)$^+$ RNA samples were separately extracted from three C57BL/6 mice and two to four WT and p53-KO mice; those samples from equivalent materials were analyzed using the Incyte GEM system and the Affymetrix system. We used the Affymetrix system to analyze further two separate RNA samples from benzene-exposed and sham-exposed WT mice at each time point, and two separate RNA samples from benzene-exposed and four separate samples from sham-exposed p53-KO mice. In addition, for further comparison, RNA samples from three mice in each of the four groups were pooled and processed with the Incyte GEM system. No duplicate or triplicate runs were performed using the Incyte GEM system. Poly(A)$^+$ RNA was prepared from the total RNA using Oligo (dT) Microbeads (Daiichi Co., Tokyo, Japan) in accordance with the manufacturer's instructions.

Microarray Preparation

All procedures such as experimental design, array design, sampling, hybridization, signal measurements, and normalization control were performed according to the MIAME (minimum information about a microarray experiment) guidelines (Brazma et al. 2001).

Affymetrix system. **Target preparation from total mRNA.** We synthesized the first-strand cDNA by incubating 40 μg total RNA with 400 U SuperScript II reverse transcriptase (Invitrogen), 100 pmol T7-$(dT)_{24}$ primer [5′-GGCCAGTGAATTGTAATACGACTCACTATAGGGAGGCGG-$(dT)_{24}$-3′], 1× first-strand cDNA synthesis buffer [50 mM Tris-HCl (pH 8.3), 75 mM KCl, 3 mM $MgCl_2$, and 10 mM dithiothreitol (DTT)], and 0.5 mM deoxynucleoside 5′-triphosphate [dNTP: mixture of 0.5 mM each deoxydenosine 5′-triphosphate (TP), deoxycytidine TP, deoxyguanosine TP, and deoxythymidine TP] at 42°C for 1 hr. We synthesized the second-strand cDNA by incubating the first-strand cDNA with 10 U *Escherichia coli* ligase (Invitrogen), 40 U DNA polymerase I (Invitrogen), 2 U RNase H (Invitrogen), 1× reaction buffer [18.8 mM Tris-HCl (pH 8.3), 90.6 mM KCl, 4.6 mM $MgCl_2$, 3.8 mM DTT, 0.15 mM nicotinamide adenine dinucleotide, and 10 mM $(NH_4)_2SO_4$], and 0.2 mM dNTP at 16°C for 2 hr. Ten units T4 DNA polymerase (Invitrogen) was added, and the reaction was allowed to continue for another 5 min at 16°C to generate the blunt-ended double-stranded (ds) cDNAs. After phenol/chloroform extraction and ethanol precipitation, the ds-cDNA was resuspended in 12 μL diethyl pyrocarbonate-treated distilled water. Biotin-labeled cRNAs were synthesized by *in vitro* transcription using a BioArray HighYield RNA transcript labeling kit (Enzo Diagnostics, Farmingdale, NY, USA). The ds-cDNA was then mixed with 1× HighYield reaction buffer, 1× mixture solution of four nucleoside TPs (NTPs: adenosine TP, cytidine TP, guanosine TP, and uridine TP) with biotin-labeled uridine TP and cytidine TP, 1× DTT, 1× RNase inhibitor mix, and 1× T7 RNA polymerase. The mixture was incubated at 37°C for 4 hr, with gentle mixing every 30 min. The labeled cRNA was then purified using an RNeasy minikit (Qiagen, Valencia, CA, USA) in accordance with manufacturer instructions. The purified cRNA was then fragmented in 1× fragmentation buffer (40 mM Tris–acetate, 100 mM potassium acetate, and 30 mM magnesium acetate) at 94°C for 35 min.

Hybridization and scanning. For hybridization, 15 μg of the fragmented cRNA probe was incubated with 50 pM control oligonucleotide B2, 1× eukaryotic hybridization control (1.5 pM *BioB*, 5 pM *BioC*, 25 pM *BioD*, and 100 pM *cre*), 0.1 mg/mL herring sperm DNA, 0.5 mg/mL acetylated bovine serum albumin, and 1× hybridization buffer in a 45°C rotisserie oven for 16 hr.

Probe array washing, staining, and antibody amplification. After hybridization, washing and staining were performed with a GeneChip fluidic station (Affymetrix) using appropriate antibody amplification washing and staining protocols.

Probe array scanning. The phycoerythrin-stained array was performed with a confocal scanner (Agilent Affymetrix GeneArray scanner), processed into digital image files, and analyzed using the Affymetrix analysis software Microarray Suite (MAS, version 4.0).

Data normalization. GeneSpring software (Silicon Genetics, Redwood City, CA, USA) was used to normalize the data. The 50th percentile of all measurements was used as a positive control for the sample; each measurement for each gene was divided by this synthetic positive control, assuming that this was at least 10. The bottom 10th percentile was used as a test for correcting background subtraction. This was never less than the negative values of the synthetic positive control. The measurement for each gene in each sample was divided by the corresponding mean of the sham controls, assuming that the cutoff value is more than 0.01.

Incyte GEM system. **Fluorescence labeling of probe for GEM system.** For comparison of the array data obtained using the Affymetrix system, the samples were simultaneously sent to the Incyte GEM system to analyze the time course of gene expression changes after benzene inhalation and its cessation. Poly(A)$^+$ RNA (200 ng) from each sample was sent to Incyte Co Ltd. (MouseUniGEM: GEM-5200; Fremont, CA, USA) via GEM custom screening services (Kurabo Co Ltd., Osaka, Japan). Briefly, the samples were incubated for 2 hr at 37°C with 200 U M-MLV reverse transcriptase (Life Technologies, Gaithersburg, MD, USA), 4 mM DTT, 1 U RNase inhibitor (Ambion, Austin, TX, USA), 0.5-mM dNTPs, and 2 μg 5′Cy3 or Cy5-labeled 9-mers (Operon Technologies Inc., Alameda, CA, USA) in 25-μL volume with an enzyme buffer supplied by the manufacturer, and then reverse-transcribed to cDNA. The reaction was terminated by heating at 85°C for 5 min. The paired reaction mixtures were combined and purified with a TE-30 column (Clonetech, Palo Alto, CA, USA), diluted to 90 μL with distilled water, and precipitated with 2 μL of 1 g/mL glycogen, 60 μL of 5 M ammonium acetate, and 300 μL ethanol. After centrifugation, the supernatant was decanted and the pellet was resuspended in 24 μL hybridization buffer, 5× sodium chlorine–sodium citrate buffer, 0.2% sodium dodecyl sulfate, and 1 mM DTT.

Hybridization. The probe solutions were thoroughly resuspended by incubating them at 65°C for 5 min, with mixing. The probe was applied to the array and covered with a 22-mm^2 glass cover slip and placed in a sealed chamber to prevent evaporation. After hybridization at 60°C for 6.5 hr, the slides were consecutively washed 3 times in a washing buffer of decreasing ionic strength.

The GEM system scanning. After hybridization, the GEM was scanned at 10-μm resolution to detect Cy3 and Cy5 fluorescence. Both Cy3 and Cy5 channels were scanned simultaneously with independent lasers. The emitted fluorescent light was optically filtered before photo-multiplier tubes translated the photons into an analog electrical signal, which was further processed into a 16-bit digital signal. This provided electronic images of both Cy3 and Cy5 with a 65,536-color resolution. A 16-color log scale was used for visual representation.

Normalization and ratio determination. Incyte GEM Tool software (Incyte) was

used for image analysis. A grid-and-region detection algorithm was used to determine the elements. The area surrounding each element image was used to calculate the local background and was subtracted from the total element signal. Background-subtracted element signals were used to calculate the Cy3:Cy5 ratio. The average of the resulting total Cy3 and Cy5 signals gives a ratio that is used to balance or normalize the signals.

Results of cDNA Microarray Analyses and Their Implications

In this study we investigated the changes in gene expression during and after benzene exposure (300 ppm). As previous studies (Yoon et al. 2001b) demonstrated that the *p53* tumor suppressor gene plays an important role in a cell response to benzene toxicity, analyses were performed using WT and p53-KO mice. In the sections that follow, we compare the gene expression profile obtained from WT mice using the Incyte GEM system with that obtained using the Affymetrix system, which in turn are compared with those of previous reports (Boley et al. 2002; Ho and Witz 1997; Schattenberg et al. 1994, Zhang et al. 2002). In addition we also describe particular genes related to p53-KO mice, such as cell cycle–regulating genes, apoptosis-related genes, and DNA repair–related genes.

All gene names, abbreviations, and accession numbers from MAS 4.0 are equivalent to those of GenBank (http://www.ncbi.nlm.nih/gov/Genbank/index.html).

Gene Expression Profile of Wild-Type Mice after Benzene Exposure

Figure 2 shows differences in the expression patterns of specific genes between, during, and after exposure of the WT mice to 300 ppm benzene for 2 weeks, determined using the Incyte GEM system (see Figure 1 for experimental schedule). Figure 2A shows the genes upregulated during benzene exposure (D5, D12), and then downregulated afterward (D+3), as represented by the *MPO* gene. Figure 2B shows the genes that had been continuously upregulated after benzene exposure, i.e., p53-binding protein 1 (*53BP1*), adenosine triphosphate (ATP)–binding cassette (ABC) transporter, and *N*-acetylglucosamine-6-*O*-sulfotransferase. Figure 2C shows the genes that had continuously been somewhat upregulated after benzene exposure, e.g., murine cathelin-like protein (*MCLP*), cell division cycle 2 (*cdc2*), and lipocalin 2. The expression patterns of *MPO* in Figure 2A may be induced by benzene metabolism during benzene exposure. This induction ceases after inhalation (Schattenberg et al. 1994), whereas *53BP1*, a DNA damage–responsive gene (Ward et al. 2003), and ABC transporter, a detoxifying drug–transporter (Ambudkar and Gottesman 1998), in Figure 2B show prolonged expressions after benzene exposure. *MCLP* (Gombert et al. 2003) and lipocalin 2 (Jessen and Stevens 2002) function as marker genes for differentiation. The genes listed in Figure 2C, including *cdc2*, may be upregulated for the proliferation of bone marrow cells during the recovery phase. A particular expression change in the aryl hydrocarbon receptor (AhR) was observed for which a mechanism could not be specified (data not shown). As we previously observed, sensitivity to benzene toxicity is innate in AhR-KO mice, implying that AhR transmits this sensitivity to benzene toxicity (Yoon et al. 2002).

The results of cDNA microarray analysis showed a broad consensus that the *p53* tumor suppressor gene is central to the mechanism of benzene action, by strictly regulating specific genes involved in the pathways of cell cycle arrest, apoptosis, and DNA repair. Such close association of the *p53* gene with the benzene toxicity mechanism raises the question: What would happen in mice whose *p53* gene is knocked out after benzene exposure? Thus, the cDNA microarray data obtained from the WT and p53-KO mice were applied to the Affymetrix system and analyzed using GeneSpring software, as described in "Materials and Methods." The results are shown in Table 1. This table shows that the expression profiles of the many genes involved in benzene metabolism, cell cycle or cell proliferation, and hemopoiesis in WT mice were generally consistent with the cDNA microarray data of C57BL/6 mice described in Table 2.

Characteristics of Gene Expression Profile of p53-KO Mice after Benzene Exposure

Mice lacking the *p53* gene and WT mice generally had similar expression patterns of the genes involved in benzene metabolism (CYP2E1 and MPO; Bernauer et al. 1999, 2000; Schattenberg et al. 1994; Yoon et al. 2001b) and hemopoiesis, suggesting that p53-KO mice are also affected to a similar extent by benzene exposure. This is consistent with the high frequency of micronuclei observed in benzene-exposed p53-deficient mice (Healy et al. 2001) (Table 1, Table 3A; p53-independent, benzene-induced gene expression level increase or decrease.). Figure 3 shows scatterplots representing the expression levels of genes in the bone marrow cells of the benzene-exposed WT (Figure 3A) and p53-KO mice (Figure 3B) relative to the expression levels of the genes in those of the corresponding sham-control mice. To elucidate and visualize the difference in gene expression level between the WT and p53-KO mice, clustering analysis was performed (Figure 4). The genes expressed include cell cycle/proliferation–associated genes. Table 3B lists the genes with a p53-dependent, benzene-induced decrease (e.g., G protein–coupled receptor [*GPCR*]) or increase (e.g., *caspase-11*) in expression level in the WT mice. In the

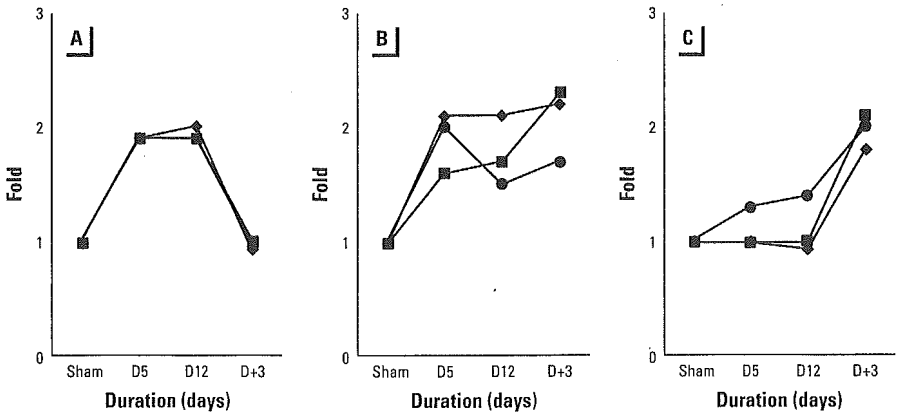

Figure 2. Three different expression patterns are shown along the time course. Benzene was used to expose the mice at 300 ppm for 1 week (D5) and 2 weeks (D12). D+3 designates the recovery group. The Incyte GEM system was used. Background-subtracted element signals were used to calculate the Cy3:Cy5 ratio. (*A*) Genes upregulated during the benzene exposure followed by immediate downregulation after benzene exposure: *MPO* (GenBank accession number X15313, [■]), *MPO* (GenBank accession number X15378, [◆]). (*B*) Genes upregulated during and after benzene exposure: *N*-acetylglucosamine-6-*O*-sulfotransferase (■), ABC transporter (◆), *53BP1* (●). (*C*) The genes were gradually or immediately upregulated after the benzene exposure, chiefly represented by DNA repair and proliferation during the recovery phase; *MCLP* (■), *cdc2* (◆), lipocalin 2 (●).